



University of Dundee

Aggregation and travelling wave dynamics in a two-population model of cancer cell growth and invasion

Bitsouni, Vasiliki; Trucu, Dumitru; Chaplain, Mark A. J.; Eftimie, Raluca

Published in:
Mathematical Medicine and Biology: a Journal of the IMA

DOI:
[10.1093/imammb/dqx019](https://doi.org/10.1093/imammb/dqx019)

Publication date:
2018

Document Version
Publisher's PDF, also known as Version of record

[Link to publication in Discovery Research Portal](#)

Citation for published version (APA):
Bitsouni, V., Trucu, D., Chaplain, M. A. J., & Eftimie, R. (2018). Aggregation and travelling wave dynamics in a two-population model of cancer cell growth and invasion. *Mathematical Medicine and Biology: a Journal of the IMA*, 1-37. [dqx019]. DOI: 10.1093/imammb/dqx019

General rights

Copyright and moral rights for the publications made accessible in Discovery Research Portal are retained by the authors and/or other copyright owners and it is a condition of accessing publications that users recognise and abide by the legal requirements associated with these rights.

- Users may download and print one copy of any publication from Discovery Research Portal for the purpose of private study or research.
- You may not further distribute the material or use it for any profit-making activity or commercial gain.
- You may freely distribute the URL identifying the publication in the public portal.

Take down policy

If you believe that this document breaches copyright please contact us providing details, and we will remove access to the work immediately and investigate your claim.

Aggregation and travelling wave dynamics in a two-population model of cancer cell growth and invasion

VASILIKI BITSOUNI AND DUMITRU TRUCU

Division of Mathematics, University of Dundee, Dundee, DD1 4HN, Scotland, UK

MARK A. J. CHAPLAIN

*School of Mathematics and Statistics, Mathematical Institute (MI), North Haugh,
University of St Andrews, St Andrews, KY16 9SS, Scotland, UK*

AND

RALUCA EFTIMIE*

Division of Mathematics, University of Dundee, Dundee, DD1 4HN, Scotland, UK

*Corresponding author. Email: reftimie@maths.dundee.ac.uk

[Received on 07 July 2016; revised on 19 September 2017; accepted on 14 November 2017]

Cells adhere to each other and to the extracellular matrix (ECM) through protein molecules on the surface of the cells. The breaking and forming of adhesive bonds, a process critical in cancer invasion and metastasis, can be influenced by the mutation of cancer cells. In this paper, we develop a nonlocal mathematical model describing cancer cell invasion and movement as a result of integrin-controlled cell–cell adhesion and cell–matrix adhesion, for two cancer cell populations with different levels of mutation. The partial differential equations for cell dynamics are coupled with ordinary differential equations describing the ECM degradation and the production and decay of integrins. We use this model to investigate the role of cancer mutation on the possibility of cancer clonal competition with alternating dominance, or even competitive exclusion (phenomena observed experimentally). We discuss different possible cell aggregation patterns, as well as travelling wave patterns. In regard to the travelling waves, we investigate the effect of cancer mutation rate on the speed of cancer invasion.

Keywords: cancer mutation; two-population mathematical model; cell–cell and cell–matrix adhesion; integrins; aggregation patterns; travelling wave patterns.

1. Introduction

Normal cells proliferate, divide and die in a highly controlled manner. This proliferation requires mitogenic signals, which are transmitted into the cell by the transmembrane receptors and bind signalling molecules, i.e. diffusible growth factors, extracellular matrix (ECM) components and cell–cell adhesion molecules (Hanahan & Weinberg, 2000). When a cell divides, its DNA is copied by the two new cells. However, if the DNA is damaged or not copied correctly, the new damaged cells will either die or start to proliferate in an uncontrolled manner, creating a signalling of oncogenes that act by mimicking growth signalling (Hanahan & Weinberg, 2000), eventually leading to an abnormal mass of tissues from cells that differ in clinically important phenotypic features (Marusyk *et al.*, 2012). More precisely, tumour formation is a result of clonal expansion driven by somatic mutation, developed by a single precursor (monoclonal) that undergoes genetic and biological changes (Khalique *et al.*, 2007; Nowell, 1976). This transformation of normal cells to cancer cells is a multistep process described via

the steps of hyperplasia, premalignant change and dysplasia (Beckmann *et al.*, 1997). Cancer cells lose their ability to regulate genome stability which leads to further genetic changes and tumour development (Khalique *et al.*, 2007). Over the last three decades it has been shown experimentally that tumours consist of heterogeneous populations of cells, which are the result of genetic instability (Stackpole, 1983; Khalique *et al.*, 2007; Loeb & Loeb, 2000; Martelotto *et al.*, 2014). Intra-tumour heterogeneity appears in almost all phenotypic cell features: from cell morphology, to gene expression, motility, proliferation, immunogenicity and metastatic potential (Nicholson, 1984, 1987; Marusyk & Polyak, 2010). It should be mentioned that also normal cells are heterogeneous for various characteristics (e.g. surface antigens). Nevertheless, cellular heterogeneity is more pronounced in malignant neoplasms (Nicholson, 1987). Since the characteristics of the most abundant cell types inside these heterogeneous tumours might not necessarily predict the properties of mixed populations (Marusyk *et al.*, 2012), we need to gain a better understanding of the dynamics of tumours formed of different mutated cell types. In fact, experimental studies have shown complex interactions between clonal sub-populations: from stable coexistence to dominant behaviours (Schuh *et al.*, 2012). For example, some studies have shown the possibility of having competitive exclusion of clonal cancer cell sub-populations in heterogeneous tumours (Leith *et al.*, 1989; Schuh *et al.*, 2012). Other studies have shown that some tumour clones can compete with alternating dominance (Keats *et al.*, 2012). We emphasize that the clonal composition of heterogeneous tumours usually changes over time (Greaves & Maley, 2012), and hence we can expect to see different competition outcomes as time increases (e.g. from transient coexistence of multiple clones to long-term competitive exclusion). Moreover, in some cancer clones there is evidence of contact domination, i.e. the inhibition of growth in some clones is the result of cell–cell contact between various cell sub-populations (Aabo *et al.*, 1994).

The metastatic and invasive potential of heterogeneous tumours is influenced by the interactions amongst cells, and the interactions between cells and the ECM, via cell surface receptors and various cytokines and chemokines. A major group of cell surface receptors is represented by the integrins, which are involved in both cell–cell adhesion and cell–matrix adhesion (Weitzman *et al.*, 1995). In particular, the successful colonization of new sites by cancer cells requires changes in integrin expression (Hanahan & Weinberg, 2000). Another group of molecules involved in cell–cell adhesion is represented by the cadherin families (Hanahan & Weinberg, 2000). The processes through which cells bind to each other and to ECM via these surface receptors, are responsible for tissue formation, stability and breakdown (Armstrong *et al.*, 2006). In particular, to detach from the main aggregation/tissue, cells loose cell–cell adhesion and strengthen cell–matrix adhesion, which leads to ECM remodelling and degradation (with the help of enzymes called matrix metalloproteinases), thus helping cell migration through the ECM (Friedl & Wolf, 2003).

Over the last 20 years, mathematical models have been used intensively to try to gain a better understanding regarding the mechanisms behind cancer invasion and metastasis or the mechanisms behind the aggregation of other types of cells (see, e.g. Ambrosi & Preziosi (2002); Andasari & Chaplain (2012); Andasari *et al.* (2011); Anderson *et al.* (2000); Armstrong *et al.* (2006); Byrne & Preziosi (2003); Chaplain *et al.* (2011); Cristini *et al.* (2009); Deakin & Chaplain (2013); Domschke *et al.* (2014); Dyson *et al.* (2016); Enderling *et al.* (2006, 2010); Gerisch & Chaplain (2008); Green *et al.* (2010); Knútsdóttir *et al.* (2014); Mogilner & Edelstein-Keshet (1995); Mogilner *et al.* (1996); Painter *et al.* (2010); Sherratt *et al.* (2009); Painter *et al.* (2015) and many references therein). The early mathematical models were described by local systems of partial differential equations incorporating some generic chemotaxis or haptotaxis mechanisms (Gerisch & Chaplain, 2008; Painter, 2009), or incorporating implicit cell–cell interactions via tumour surface forces (Byrne & Chaplain, 1996). For example, Anderson *et al.* (2000) developed a local Partial Differential Equations (PDE) model of

parabolic type for the invasion of cancer cells via cell–matrix interactions that lead to ECM degradation. [Byrne & Chaplain \(1996\)](#) modelled phenomenologically the influence of cell adhesion on tumour growth, by considering surface forces on tumour spheroids. As it became more clear that the movement in response to chemical/haptotactic gradients was facilitated by the binding and unbinding of cell surface molecules to other cells and to ECM, new mathematical models of parabolic type have been derived to describe these cell–cell and cell–matrix adhesion processes ([Armstrong *et al.*, 2006](#); [Dyson *et al.*, 2016](#); [Gerisch & Chaplain, 2008](#); [Gerisch & Painter, 2010](#); [Green *et al.*, 2010](#); [Painter *et al.*, 2015](#)). Since these models incorporate the assumption that cells at position \mathbf{x} bind/unbind to/from other cells at position $\mathbf{x} \pm \mathbf{s}$ (for some $s > 0$ within cells sensing radius), they are generally nonlocal. For example, [Armstrong *et al.* \(2006\)](#) focused on cell movements due to cell–cell adhesion, and introduced a nonlocal term that described the nature, the direction, as well as the strength of the adhesive forces between cancer cells. The authors also extended the nonlocal model to two populations that interact via adhesive forces (thus incorporating self-population and cross-population adhesion), and studied the effect of different adhesion strengths on the sorting or the mixing of cell populations. A similar two-population nonlocal model of parabolic type, which incorporated also cell proliferation and cell movement in response to cell ‘packing’, was described and investigated by [Painter *et al.* \(2015\)](#). The model in [Armstrong *et al.* \(2006\)](#) was further generalized by [Gerisch & Chaplain \(2008\)](#), [Painter *et al.* \(2010\)](#), [Domschke *et al.* \(2014\)](#) to include also cell–matrix interactions. While the majority of these models investigated cell–cell and cell–matrix adhesion in one cell population, a few models considered also multiple interacting cell populations ([Domschke *et al.*, 2014](#)). In particular, [Domschke *et al.* \(2014\)](#) also assumed mutation between different cell populations. A different class of nonlocal models for cancer invasion has been developed in the context of the velocity-jump framework introduced in [Othmer *et al.* \(1988\)](#) and the kinetic models for active particles framework described, e.g. in [Bellomo *et al.* \(2010\)](#); see the transport models in [Kelkel & Surulescu \(2012\)](#), [Lorenz & Surulescu \(2014\)](#), [Engwer *et al.* \(2015, 2017\)](#), [Hunt & Surulescu \(2017\)](#).

We should emphasize here that all these nonlocal models for cell invasion are variations or generalizations of nonlocal models developed over the last two decades to describe the dynamics of cell populations ([Edelstein-Keshet & Ermentrout, 1990](#)), bacterial populations ([Othmer *et al.*, 1988](#); [Xue *et al.*, 2011](#); [Perthame *et al.*, 2016](#)) or the dynamics of self-organized animal populations ([Mogilner & Edelstein-Keshet, 1999](#); [Topaz *et al.*, 2006](#); [Eftimie *et al.*, 2007](#); [Fetecau & Eftimie, 2010](#); [Carrillo de la Plata *et al.*, 2015](#); [Fetecau, 2011](#)). While the models describing collective cell movement are usually of parabolic type, the latest models for collective bacterial movement and collective animal movement are usually of hyperbolic/transport type.

In this study, we will investigate the role of cancer mutation on the possibility of clonal competition with alternating dominance or even competitive exclusion between two cancer cell sub-populations (as discussed before, these types of competition have been observed experimentally ([Leith *et al.*, 1989](#); [Keats *et al.*, 2012](#); [Schuh *et al.*, 2012](#))). To this end, we will introduce a nonlocal model for cell–cell and cell–matrix adhesion for two populations of cells (this model is a generalization of the models in [Armstrong *et al.* \(2006\)](#); [Gerisch & Chaplain \(2008\)](#); [Painter *et al.* \(2015\)](#)). However, in contrast to these previous models which are of parabolic type, here we consider a parabolic–hyperbolic model. More precisely, we assume that one ‘normal’ cancer cell population moves both randomly and in a directed manner in response to cell–cell and cell–matrix adhesive forces, while a second ‘mutant’ cancer cell population (i.e. a mutated clone) moves predominantly in a directed manner following cell–cell interactions (with cells from both populations) and cell–matrix interactions (as suggested by experimental observations in [Goswami *et al.* \(2005\)](#); [Hagemann *et al.* \(2005\)](#)). By incorporating this assumption, we aim to bring a more realistic approach to the models since the various intra-tumour cell

sub-populations have been shown to be distinct not only in their adhesion capabilities but also in their motility and metastatic potential (Marusyk & Polyak, 2010). Moreover, we are interested in investigating the effect of mutation on the spreading speed of the mutated cancer cells, since the invasion levels of the mutant cancer cells are higher compared to those of ‘normal’ cancer cells (Chapman *et al.*, 2014; Wojciechowska & Patton, 2015). Also, while previous nonlocal models have assumed constant adhesive interactions, here we will assume that these adhesive interactions depend on the level of integrins. Note that instead of assuming a kinetic (mesoscale) approach for cell-dependence on integrins as in Lorenz & Surulescu (2014), Engwer *et al.* (2015), Perthame *et al.* (2016), Engwer *et al.* (2017), Hunt & Surulescu (2017), here we follow a microscale–macroscale approach similar to Stinner *et al.* (2014, 2015, 2016) and Meral *et al.* (2015a,b) and couple the parabolic–hyperbolic model for spatial cell dynamics with an Ordinary Differential Equation (ODE) for integrins dynamics. We then investigate this complex multiscale model in terms of pattern formation, with particular attention being paid to the role of mutation rate on the coexistence (or not) of cell sub-populations that form stationary aggregations or travelling wave patterns.

The layout of this paper is as follows. In Section 2 we formulate a model of partial integro-differential equations for the dynamics of two cancer cell populations, coupled with ordinary differential equations describing ECM and integrins dynamics. In Section 3 we use linear stability analysis to investigate the ability of the model to form cell aggregations. In Section 4 we investigate numerically some types of spatio-temporal patterns exhibited by this nonlocal model. In Section 5 we investigate numerically and analytically travelling wave behaviours. We conclude in Section 6 with a summary and discussion of the results.

2. A mathematical model of two cancer cell sub-populations

2.1 Derivation of the model

Cancer invasion is a complex process involving cell–cell interactions, and interactions between cells and non-cellular components (Calvo & Sahai, 2011). To develop our model we consider two populations of cancer cells, a ‘normal’ (original clone) cancer population and a ‘mutant’ (descendant clone) population, which interact with each other as well as with the ECM via long-range adhesive and repulsive forces (Demant *et al.*, 1976; Geiger, 1991); see Fig. 1.

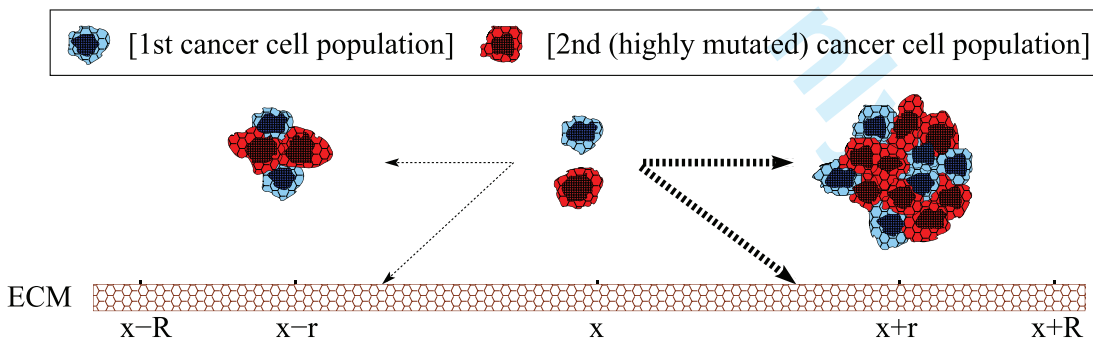


FIG. 1. A caricature illustration of movement decisions made by cells at x , following interactions with neighbouring cells at $x - r$ and $x + r$, and with the ECM. For very strong attraction (represented here by thicker arrows), cells move towards larger cell aggregations.

Let $\Omega \subset \mathbb{R}^d$ denote a bounded spatial domain (here we consider only $d = 1$; for a 2D version of the model see Appendix A), with periodic boundary conditions. Let $I_T = [0, \infty)$ be the time interval. Denote by $u_1(x, t)$ the density of ‘normal’ cancer cells at position x and time t , and by $u_2(x, t)$ the density of ‘mutant’ cancer cells at position x and time t . We also denote by $f(x, t)$ the ECM density, and by $c(x, t)$ the density of integrin receptors on the surface of cancer cells (receptors involved in cell–cell and cell–matrix interactions). For compact notation, we define the vectors $\underline{u}(x, t) = (u_1(x, t), u_2(x, t))^T$ and $\underline{v}(x, t) = (\underline{u}(x, t), f(x, t))^T$.

DYNAMICS OF CANCER CELLS. Experimental studies (Chapman *et al.*, 2014) have shown that cancer cells can switch from a homogeneous type of invasion to a heterogeneous type of invasion described by invading chains (Chapman *et al.*, 2014; Friedl & Wolf, 2003; Wojciechowska & Patton, 2015). Here, we assume that u_1 cells can mutate into u_2 cells at a constant rate M . We can derive a model for heterogeneous cancer cell populations by considering the equations

$$\frac{\partial u_i}{\partial t} = -\frac{\partial J_i}{\partial x} + (-1)^i M u_1 + G_i(\underline{u}), \quad i = 1, 2, \quad (2.1)$$

where J_i , $i = 1, 2$, are the cell fluxes and $G_i(\underline{u})$, $i = 1, 2$, are the growth functions of populations u_i , $i = 1, 2$. The fluxes describe the factors that define cell movement. In this study we assume that the movement of the ‘normal’ cancer cell population u_1 is governed by random motility (which underlines a homogeneous type of invasion), as well as directed motility in response to cell–cell and cell–matrix adhesive forces (which underlines the heterogeneous type of invasion) (Calvo & Sahai, 2011). In contrast, the ‘mutant’ u_2 cell population moves only in a directed manner (hence exhibiting an heterogeneous type of invasion) in response to cell–cell and cell–matrix adhesion forces. Biologically, this directed movement of ‘mutant’ (more invasive) cancer cells can be explained by the increase of macrophage density near highly mutated cancer cells (Lin *et al.*, 2006), which promotes the directed movement and invasion of these cancer cells, and decreases their random movement (Goswami *et al.*, 2005; Hagemann *et al.*, 2005). Therefore, in this study we assume that the movement of u_2 population due to random walk can be considered negligible. In this case, the total fluxes will be

$$J_1 = J_D + J_{a_1} \quad \text{and} \quad J_2 = J_{a_2}, \quad (2.2)$$

where J_D is the flux due to Fickian diffusion, given by $J_D = -D\partial u_1/\partial x$, with D to be the diffusion coefficient, and J_{a_i} , $i = 1, 2$, are the adhesive fluxes for cell–cell and cell–matrix adhesion. In the case of u_2 the diffusion is considered very small and thus we ignore it.

Cell–cell/cell–matrix adhesion–mediated directed cancer cell migration occurs as a result of the social forces, i.e. attraction and repulsion, between cells and between cells and ECM components, when adhesive bonds are formed and broken. Cell–cell adhesion is described as the adhesion between cells of the same population, as well as cross-adhesion between cells of the two sub-populations. The cell–cell/cell–matrix adhesion forces are created through the binding of adhesion molecules, e.g. integrins, at cell surface. To model these forces, let us define $R > 0$ to be the sensing radius of the cells, i.e. the maximum range over which cells can detect other surrounding cells, which biologically represent the extent of the cell protrusions (e.g. filopodia) (Armstrong *et al.*, 2006). Let $g_i(\underline{v}(x+r, t), c(x, t))$, $i = 1, 2$, describe the nature of the cell–cell and cell–matrix adhesive forces created at x due to signalling

with cell/ECM components at $x + r$. These functions increase when the cell density and ECM density increase, and accordingly they decrease when the cell density and ECM density decrease. The functions g_i , $i = 1, 2$, are chosen as in Bitsouni *et al.* (2017) to be given by

$$g_1(\underline{v}(x+r, t), c(x, t)) := S_1(c(x, t))u_1(x+r, t) + S(c(x, t))u_2(x+r, t) + C_1(c(x, t))f(x+r, t), \quad (2.3)$$

and

$$g_2(\underline{v}(x+r, t), c(x, t)) := S_2(c(x, t))u_2(x+r, t) + S(c(x, t))u_1(x+r, t) + C_2(c(x, t))f(x+r, t), \quad (2.4)$$

where $S_i(c(x, t))$ is the cell–cell self-adhesion strength function for populations u_i , $S(c(x, t))$ is the cell–cell cross-adhesion strength function between the two populations, and $C_i(c(x, t))$ is the adhesion strength function between population u_i and ECM. We should mention here that a similar term was considered before by Chaplain *et al.* (2011). Other studies (Armstrong *et al.*, 2006; Gerisch & Chaplain, 2008) consider volume filling effect to avoid unbounded aggregations. While unbounded aggregations are possible in this type of nonlocal models, these have not been observed in our system (at least not for the parameter ranges used in this study).

We define these adhesion strength functions in terms of the integrin density c : the more integrins a cell has, the stronger its adhesion force (Gallant *et al.*, 2005). However, the adhesion strength reaches a plateau for a large integrin density (Maheshwari *et al.*, 2000). Thus, we require an increasing, bounded function, so that we avoid extreme phenomena for large values of integrin density. A biologically realistic choice is a sigmoid function. This choice is supported by various other experimental studies in the literature which have shown that different biological processes can be described by sigmoid functions: from cell adhesion via integrins (Cutler & García, 2003; Michael *et al.*, 2009), to oxygen saturation (Shiao & Ou, 2007). Note also that since cell mutation could lead to more integrins (Kidera *et al.*, 2010), we consider strength functions with different integrin levels for each of the two populations. To this end, we choose the adhesion strength functions to be given by:

$$\begin{aligned} S_1(c) &= s_1^* (1 + \tanh(a_1c)), \quad S_2(c) = s_2^* (1 + \tanh(a_2c)), \quad S(c) = s^* (1 + \tanh(dc)), \\ C_1(c) &= c_1^* (1 + \tanh(b_1c)), \quad C_2(c) = c_2^* (1 + \tanh(b_2c)), \end{aligned} \quad (2.5)$$

where $d, a_i, b_i, i = 1, 2$, and $s^*, s_i^*, c_i^*, i = 1, 2$, are positive real numbers.

Within this sensing radius, let us now define K_{cc} and K_{cm} , the kernels for cell–cell and cell–matrix adhesion ranges, respectively:

$$K_{cc}(r) = \begin{bmatrix} K_{11}(r) & K_{12}(r) \\ K_{21}(r) & K_{22}(r) \end{bmatrix}, \quad K_{cm}(r) = \begin{bmatrix} K_1(r) \\ K_2(r) \end{bmatrix}.$$

These interaction kernels describe the dependency of the force magnitude on the distance r from x . Here K_{ij} , $i, j = 1, 2$, are the interaction kernels between population i and population j (i.e. cell–cell

interactions), and K_i , $i = 1, 2$, are the kernels for cell–matrix interactions (for the two populations). For simplicity, throughout this study we will consider (see also [Domschke et al., 2014](#)):

$$K_{11} = K_{12} = K_1 \text{ and } K_{22} = K_{21} = K_2. \tag{2.6}$$

Moreover, we assume that these kernels are attractive at medium/long ranges (i.e. at the edges of the cell) and repulsive at very short ranges (i.e. over cell surface), and thus can be defined as

$$K_{1,2}(r) := q_a K_a^{1,2}(r) - q_r K_r^{1,2}(r), \tag{2.7}$$

with q_a and q_r describing the magnitudes of attractive and repulsive interactions, and $K_a^{1,2}(r)$ and $K_r^{1,2}(r)$ describing the spatial ranges over which these interactions take place. We will discuss various examples of attractive (K_a) and repulsive (K_r) kernels in Section 3, in the context of linear stability analysis.

Therefore, the local cell–cell and cell–matrix adhesion forces will be described by the product of functions g_i and $K_i(r)$, $i = 1, 2$. To describe the nonlocal cell–cell and cell–matrix adhesion and repulsion forces ([Deman et al., 1976](#); [Geiger, 1991](#)), we sum all such forces by integrating over space to obtain the total forces:

$$F_1[\underline{u}, f, c](x, t) := \frac{1}{R} \int_0^R \sum_{k=0}^1 \eta(k) K_1(r) g_1(\underline{u}(x + r\eta(k), t), c(x, t)) \, dr, \tag{2.8}$$

and

$$F_2[\underline{u}, f, c](x, t) := \frac{1}{R} \int_0^R \sum_{k=0}^1 \eta(k) K_2(r) g_2(\underline{u}(x + r\eta(k), t), c(x, t)) \, dr, \tag{2.9}$$

where $\eta(k) = (-1)^k$, $k = 0, 1$, is the direction of the forces. Thus, the full nonlocal interaction terms are described by

$$\begin{aligned} F_1[\underline{u}, f, c](x, t) &= \frac{1}{R} \int_0^R \sum_{k=0}^1 \eta(k) K_1(r) [S_1(c) u_1(x + r\eta(k), t) + S(c) u_2(x + r\eta(k), t)] \, dr \\ &\quad + \frac{1}{R} \int_0^R \sum_{k=0}^1 \eta(k) K_1(r) C_1(c) f(x + r\eta(k), t) \, dr, \end{aligned} \tag{2.10}$$

and

$$\begin{aligned} F_2[\underline{u}, f, c](x, t) &= \frac{1}{R} \int_0^R \sum_{k=0}^1 \eta(k) K_2(r) [S_2(c) u_2(x + r\eta(k), t) + S(c) u_1(x + r\eta(k), t)] \, dr \\ &\quad + \frac{1}{R} \int_0^R \sum_{k=0}^1 \eta(k) K_2(r) C_2(c) f(x + r\eta(k), t) \, dr. \end{aligned} \tag{2.11}$$

We assume that the adhesive fluxes are proportional to the density of the cells and the nonlocal adhesion forces, F_i , $i = 1, 2$. Thus, we obtain the following expressions for the two adhesive fluxes:

$$J_{a_i} = u_i F_i[\underline{u}, f, c], \quad i = 1, 2. \quad (2.12)$$

Substituting (2.12) into the general mass conservation equations, we have the following equations describing the dynamics of the two cancer cell populations:

$$\frac{\partial u_1}{\partial t} = D \frac{\partial^2 u_1}{\partial x^2} - \frac{\partial}{\partial x} (u_1 F_1[\underline{u}, f, c]) - M u_1 + G_1(\underline{u}), \quad (2.13a)$$

$$\frac{\partial u_2}{\partial t} = - \frac{\partial}{\partial x} (u_2 F_2[\underline{u}, f, c]) + M u_1 + G_2(\underline{u}). \quad (2.13b)$$

We assume that both u_1 and u_2 cells can proliferate in a logistic manner (to describe the observed slow-down in tumour growth following the loss of nutrients (Laird, 1964)). Thus, the growth functions are given by

$$G_i(\underline{u}) = r_i u_i \left(1 - \frac{u_1 + u_2}{k_u} \right), \quad i = 1, 2, \quad (2.14)$$

where r_1 and r_2 are the growth rates of the u_1 and u_2 populations, respectively, and k_u is the carrying capacity. Note that these growth functions incorporate also the principle of competition between clonal sub-populations in heterogeneous tumours (Leith *et al.*, 1989).

ECM DYNAMICS. Cancer cell populations degrade the ECM upon contact. Moreover, ECM density is remodelled back to normal levels by cancer and healthy cells. Thus, the dynamics of ECM, $f(x, t)$, can be described by:

$$\frac{\partial f}{\partial t} = -\alpha u_1 f - \beta u_2 f + \gamma \left(1 - \frac{u_1 + u_2}{k_u} - \frac{f}{f_m} \right), \quad (2.15)$$

where α and β are the positive rate constants of ECM degradation by u_1 and u_2 cell populations, respectively, k_u is the carrying capacity of the cancer cell populations and f_m is the maximum ECM density at which the ECM fills up all available physical space. Following the approach of Anderson *et al.* (2000); Gerisch & Chaplain (2008), we choose to ignore the ECM remodelling terms for this model, i.e. we always use $\gamma = 0$.

INTEGRIN DYNAMICS. We assume that the level of integrins depends on cancer cell density. Moreover, we assume that cell mutation changes the density of receptors (since in highly metastatic cancers, the expression of integrins is up-regulated (Kidera *et al.*, 2010)). We follow an approach similar to (Stinner *et al.*, 2014, 2015, 2016; Meral *et al.*, 2015a,b) and assume that the dynamics of integrins $c(x, t)$ can be described by an ODE:

$$\frac{\partial c}{\partial t} = p_1 u_1 + p_2 u_2 - q c, \quad (2.16)$$

where q is the decay rate of c , and p_1 and p_2 are the production rates of integrins by population u_1 and u_2 , respectively. To model the increase in receptors on mutant cancer cells, we assume that $p_2 > p_1$ (see Table 2). Note that integrins are produced at the positions where these cells exist, and as cells move to different spatial positions the integrins will be produced at these new positions, too (this can be seen more clearly in Figs 4–10). Moreover, the production of integrins at various positions in space is counterbalanced by the decay term ($-qc$), which ensures that integrins will be removed from regions where cells do not exist.

For the initial conditions, we start with only population $u_1(x, 0) = u_1^0(x)$. The second population u_2 , arises from mutations in the population u_1 after a period of time, and thus $u_2(x, 0) = 0$. For the ECM, we assume that the tumour has already degraded some of its surrounding tissues:

$$f(x, 0) = 1 - 0.5u_1(x, 0) - 0.5u_2(x, 0). \quad (2.17)$$

Finally, the integrin density, c , is proportional to the initial tumour cell density

$$c(x, 0) = 0.5u_1(x, 0) + 0.5u_2(x, 0). \quad (2.18)$$

To complete our model we need to impose boundary conditions. Throughout this study we assume that the two cancer cell populations move on a circular finite domain of length L , i.e. $x \in [0, L]$. The periodic boundary conditions that model this movement are

$$u_1(0, t) = u_1(L, t) \text{ and } u_2(0, t) = u_2(L, t). \quad (2.19)$$

Note that with this choice of boundary condition, the nonlocal terms are wrapped around the domain. We will return to this aspect in Section 4.

REMARK 2.1 Note that equations (2.13)–(2.16) describe a ‘microscale–macroscale’ model, where the spatially-averaged microscale integrin dynamics (described by an ODE) is coupled with the spatial dynamics of cancer cells (described by nonlocal PDEs). As mentioned above, this modelling approach follows various other recent studies on cancer cell–matrix adhesion via integrins (Stinner *et al.*, 2014, 2015, 2016; Meral *et al.*, 2015a,b). Moreover, the coupling of PDEs for cell movement with ODEs for the dynamics of cell receptors has been considered not only for cancer cells but also for other types of cells, such as ‘Dictyostelium’ cells (Höfer *et al.*, 1995a,b). However, the past 10–15 years have seen the development of structured cell population models (described by ‘mesoscale’ models) where the macroscopic cell dynamics is dependent on a microscopic variable that characterizes the cells at molecular level (Erban & Othmer, 2004, 2005; Xue *et al.*, 2011; Lorenz & Surulescu, 2014; Engwer *et al.*, 2015; Perthame *et al.*, 2016; Engwer *et al.*, 2017; Hunt & Surulescu, 2017). In Appendix B we present a modified mesoscale version of model (2.13)–(2.16) where we assume that the two cancer cell populations are structured by an internal variable that describes the integrin level. (Here we use the terminology of ‘mesoscale’ and ‘microscale–macroscale’ models in the same spirit as Stinner *et al.* (2014), Lorenz & Surulescu (2014) and Hunt & Surulescu (2017).)

2.2 Non-dimensionalization of the model

To non-dimensionalize system (2.13) and equations (2.15)–(2.16), we define the following quantities:

$$\begin{aligned} \tilde{t} &= \frac{t}{\tau}, \quad \tilde{x} = \frac{x}{L_0}, \quad \tilde{u}_1 = \frac{u_1}{k_u}, \quad \tilde{u}_2 = \frac{u_2}{k_u}, \quad \tilde{f} = \frac{f}{f_m}, \quad \tilde{c} = \frac{c}{c_m}, \quad \tilde{R} = \frac{R}{L_0}, \quad \tilde{r} = \frac{r}{L_0}, \\ \tilde{S}(\tilde{c}) &= \frac{\tau k_u}{L_0^2} S(c_m \tilde{c}), \quad \tilde{S}_i(\tilde{c}) = \frac{\tau k_u}{L_0^2} S_i(c_m \tilde{c}), \quad \tilde{C}_i(\tilde{c}) = \frac{\tau f_m}{L_0^2} C_i(c_m \tilde{c}), \quad i = 1, 2. \end{aligned} \quad (2.20)$$

Here, L_0 is a length scale, defined as the maximum invasion distance of the cancer cells at the ‘normal’ of invasion (Anderson *et al.*, 2000). Usually L_0 is in the range of 0.1–1 cm. We rescale time with $\tau := L_0^2/D_\tau$, where D_τ is the characteristic diffusion coefficient ($\sim 10^{-6}\text{cm}^2\text{s}^{-1}$). In addition, we rescale the cancer cells, the ECM and the integrins with k_u, f_m and c_m , respectively. Here k_u is the carrying capacity of the cancer cell populations and it is taken to be $\sim 6.7 \cdot 10^7$ cell/volume, and f_m is the maximum ECM density at which the ECM fills up all available physical space and it is taken to be equal to 4 mg/volume, as in Domschke *et al.* (2014). Finally, c_m is the maximum integrin density and it is taken to be $5 \cdot 10^4$ integrins per cell (as in Benedetto *et al.* (2006)). For the kernels $K_i(r), i = 1, 2$, we choose (as in Domschke *et al.* (2014)) the dimensionless functions $\tilde{K}_i(\tilde{r}), i = 1, 2$, given by

$$\tilde{K}_i(\tilde{r}) := L_0 K_i(L_0 \tilde{r}) = L_0 K_i(r), \quad i = 1, 2.$$

We define the dimensionless functions $\tilde{g}_i(\tilde{u}, \tilde{f}, \tilde{c}), i = 1, 2$, by

$$\tilde{g}_i(\tilde{u}, \tilde{f}, \tilde{c}) := \frac{\tau}{L_0^2} g_i(u, f, c), \quad i = 1, 2.$$

Therefore, we have for the nonlocal terms $F_i[u, f, c], i = 1, 2$, that

$$\tilde{F}_i[\tilde{u}, \tilde{f}, \tilde{c}] := \frac{\tau}{L_0} F_i[u, f, c], \quad i = 1, 2.$$

Finally, we obtain the dimensionless parameters:

$$\tilde{D} = \frac{D}{D_\tau}, \quad \tilde{M} = \tau M, \quad \tilde{\alpha} = \tau \alpha k_u, \quad \tilde{\beta} = \tau \beta k_u, \quad \tilde{q} = \tau q, \quad \tilde{r}_i = \tau r_i, \quad \tilde{p}_i = \frac{\tau p_i k_u}{c_m}, \quad i = 1, 2. \quad (2.21)$$

After dropping the tildes for notational convenience, we obtain the following non-dimensionalized system

$$\frac{\partial u_1}{\partial t} = D \frac{\partial^2 u_1}{\partial x^2} - \frac{\partial}{\partial x} (u_1 F_1[u, f, c]) - M u_1 + r_1 u_1 (1 - u_1 - u_2), \quad (2.22a)$$

$$\frac{\partial u_2}{\partial t} = - \frac{\partial}{\partial x} (u_2 F_2[u, f, c]) + M u_1 + r_2 u_2 (1 - u_1 - u_2), \quad (2.22b)$$

$$\frac{\partial f}{\partial t} = -\alpha u_1 f - \beta u_2 f, \quad (2.22c)$$

$$\frac{\partial c}{\partial t} = p_1 u_1 + p_2 u_2 - qc. \quad (2.22d)$$

From now on, we will always refer to the non-dimensional quantities. In the next two sections, we discuss the dynamics of model (2.22).

3. Linear stability analysis of the model

Next, we investigate the conditions under which the two populations of cancer cells form aggregations. We first calculate the spatially homogeneous steady states of the model, and then apply standard linear stability analysis to investigate the conditions (for parameter values) under which the two cancer cell populations can form aggregations.

To start, we look for the homogeneous steady states of the ODE model associated to system (2.22), that describes the growth and mutation of the two cancer cell populations and the temporal dynamics of ECM and integrins (i.e. no spatial movement):

$$\frac{\partial u_1}{\partial t} = -Mu_1 + r_1 u_1 (1 - u_1 - u_2) = 0, \quad (3.1a)$$

$$\frac{\partial u_2}{\partial t} = Mu_1 + r_2 u_2 (1 - u_1 - u_2) = 0, \quad (3.1b)$$

$$\frac{\partial f}{\partial t} = -\alpha u_1 f - \beta u_2 f = 0, \quad (3.1c)$$

$$\frac{\partial c}{\partial t} = p_1 u_1 + p_2 u_2 - qc = 0, \quad (3.1d)$$

which has the following steady state solutions (u_1^*, u_2^*, f^*, c^*) :

$$(0, 0, f^*, 0) \text{ and } \left(0, 1, 0, \frac{p_2}{q}\right), \quad (3.2)$$

with $f^* \geq 0$. Here we consider only the non-negative solutions, since we require biological realism. Note that all these homogeneous steady states have $u_1 = 0$ (so the more invasive population u_2 persists longer). However, as we will see in Section 4, the model can exhibit non-homogeneous steady states with $u_1(x, t) \neq 0$.

We now investigate the stability of the steady states for the spatially homogeneous and spatially heterogeneous systems, to see if the introduction of spatial dynamics (i.e. cell movement and cell-cell/matrix adhesion) can lead to instabilities. First, we substitute the steady states (3.2) into

the Jacobian matrix of the spatially homogeneous system (3.1) and calculate the four eigenvalues corresponding to each steady state. Thus, for the steady state $(0, 0, f^*, 0)$ we have the eigenvalues

$$\lambda_1 = 0, \quad \lambda_2 = -M + r_1, \quad \lambda_3 = r_2 > 0 \text{ and } \lambda_4 = -q < 0. \quad (3.3)$$

Since $\lambda_3 > 0$, this state is unstable. For the steady state $(0, 1, 0, p_2/q)$ we obtain the eigenvalues

$$\lambda_1 = -\beta < 0, \quad \lambda_2 = -M < 0, \quad \lambda_3 = -r_2 < 0 \text{ and } \lambda_4 = -q < 0. \quad (3.4)$$

Since all eigenvalues are negative, the state $(0, 1, 0, p_2/q)$ is always linearly stable to homogeneous perturbations.

Next, we investigate the linear stability analysis of the spatial system (2.22). To this end, we apply small spatial perturbations to the previous homogeneous steady states: $u_i(x, t) = u_i^* + \bar{u}_i(x, t)$, $i = 1, 2$, $f(x, t) = f^* + \bar{f}(x, t)$, $c(x, t) = c^* + \bar{c}(x, t)$, where $\bar{u}_1, \bar{u}_2, \bar{f}$ and \bar{c} denote the small perturbations. (Note that, to avoid negative solutions when we perturb the zero steady states, we consider $\bar{u}_1(x, t), \bar{u}_2(x, t), \bar{f}(x, t), \bar{c}(x, t) \geq 0$.) Substituting these into the system (2.22) (after the adhesion strength functions $S_i(c), S(c), C_i(c), i = 1, 2$, have been expanded in Taylor series), and ignoring non-linear terms, leads to the following linearized system:

$$\begin{aligned} \frac{\partial \bar{u}_1}{\partial t} = & D \frac{\partial^2 \bar{u}_1}{\partial x^2} - \frac{u_1^*}{R} \frac{\partial}{\partial x} \left\{ \int_0^R K_1(r) S_1(c^*) (\bar{u}_1(x+r, t) - \bar{u}_1(x-r, t)) \, dr \right\} \\ & - \frac{u_1^*}{R} \frac{\partial}{\partial x} \left\{ \int_0^R K_1(r) [S(c^*) (\bar{u}_2(x+r, t) - \bar{u}_2(x-r, t)) + C_1(c^*) (\bar{f}(x+r, t) - \bar{f}(x-r, t))] \, dr \right\} \\ & - M \bar{u}_1 + r_1 \bar{u}_1 (1 - 2u_1^* - u_2^*) - r_1 u_1^* \bar{u}_2, \end{aligned} \quad (3.5a)$$

$$\begin{aligned} \frac{\partial \bar{u}_2}{\partial t} = & - \frac{u_2^*}{R} \frac{\partial}{\partial x} \left\{ \int_0^R K_2(r) [S_2(c^*) (\bar{u}_2(x+r, t) - \bar{u}_2(x-r, t)) + S(c^*) (\bar{u}_1(x+r, t) - \bar{u}_1(x-r, t))] \, dr \right\} \\ & - \frac{u_2^*}{R} \frac{\partial}{\partial x} \left\{ \int_0^R K_2(r) C_2(c^*) (\bar{f}(x+r, t) - \bar{f}(x-r, t)) \, dr \right\} + M \bar{u}_1 + r_2 \bar{u}_2 (1 - u_1^* - 2u_2^*) - r_2 u_2^* \bar{u}_1, \end{aligned} \quad (3.5b)$$

$$\frac{\partial \bar{f}}{\partial t} = -\alpha (\bar{u}_1 f^* + u_1^* \bar{f}) - \beta (\bar{u}_2 f^* + u_2^* \bar{f}), \quad (3.5c)$$

$$\frac{\partial \bar{c}}{\partial t} = p_1 \bar{u}_1 + p_2 \bar{u}_2 - q \bar{c}. \quad (3.5d)$$

We look for solutions of the form $A_{u_1} e^{ikx+\lambda t}$, $A_{u_2} e^{ikx+\lambda t}$, $A_f e^{ikx+\lambda t}$ and $A_c e^{ikx+\lambda t}$ with $|A_{u_1}|, |A_{u_2}|, |A_f|, |A_c| \ll 1$, where k and λ are the wave number and frequency, respectively. Then system (3.5) reduces to

$$\lambda A_{u_1} = -k^2 D A_{u_1} + \frac{2k u_1^*}{R} [S_1(c^*) A_{u_1} + S(c^*) A_{u_2} + C_1(c^*) A_f] \hat{K}_1^s(k) - M A_{u_1} + r_1 A_{u_1} (1 - 2u_1^* - u_2^*) - r_1 u_1^* A_{u_2}, \tag{3.6a}$$

$$\lambda A_{u_2} = \frac{2k u_2^*}{R} [S_2(c^*) A_{u_2} + S(c^*) A_{u_1} + C_2(c^*) A_f] \hat{K}_2^s(k) + M A_{u_1} + r_2 A_{u_2} (1 - u_1^* - 2u_2^*) - r_2 u_2^* A_{u_1}, \tag{3.6b}$$

$$\lambda A_f = -\alpha (A_{u_1} f^* + u_1^* A_f) - \beta (A_{u_2} f^* + u_2^* A_f), \tag{3.6c}$$

$$\lambda A_c = p_1 A_{u_1} + p_2 A_{u_2} - q A_c, \tag{3.6d}$$

where $\hat{K}_{1,2}^s(k) = \int_0^R K_{1,2}(r) \sin(kr) dr$ are the Fourier sine transforms of the kernels $K_{1,2}(r)$. For simplicity, throughout the rest of this study, we will assume that $K_1(r) = K_2(r) =: K(r)$ and thus $\hat{K}_1^s(k) = \hat{K}_2^s(k) =: \hat{K}^s(k)$.

Cellular aggregations form when the steady states (u_1^*, u_2^*, f^*, c^*) are unstable to spatial perturbations, and for this to happen we require the maximum real part of eigenvalues of the Jacobian matrix of system (3.6) to be positive, for at least one discrete value of $k > 0$.

- For the state $(u_1^*, u_2^*, f^*, c^*) = (0, 0, f^*, 0)$ we obtain the eigenvalues

$$\lambda_1 = 0, \quad \lambda_2 = -k^2 D - M + r_1, \quad \lambda_3 = r_2 > 0, \quad \lambda_4 = -q < 0. \tag{3.7}$$

Thus, the steady state $(u_1^*, u_2^*, f^*, c^*) = (0, 0, f^*, 0)$ is unstable.

- For the state $(u_1^*, u_2^*, f^*, c^*) = (0, 1, 0, p_2/q)$ we obtain the eigenvalues

$$\lambda_1 = -\beta < 0, \quad \lambda_2 = -k^2 D - M < 0, \quad \lambda_3 = S_2(c^*) Y(k) - r_2, \quad \lambda_4 = -q < 0, \tag{3.8}$$

where $Y(k) = \frac{2k}{R} \hat{K}^s(k)$. Recall that in the absence of diffusion and advection, the steady state $(u_1^*, u_2^*, f^*, c^*) = (0, 1, 0, p_2/q)$ is linearly stable. Thus, for aggregation to form, we require this state to be unstable to spatially inhomogeneous perturbations (Benson *et al.*, 1993), i.e. the maximum real part of the eigenvalues to be greater than zero. Since $\lambda_1, \lambda_2, \lambda_4 < 0$, the steady state $(0, 1, 0, p_2/q)$ is unstable if the following dispersion relation holds:

$$Re(\lambda_3(k)) = Re\left(-r_2 + \frac{2k s_2^*}{R} \left(1 + \tanh\left(a_2 \frac{p_2}{q}\right)\right) \hat{K}^s(k)\right) > 0. \tag{3.9}$$

We notice that this dispersion relation, and therefore the possibility of cell aggregations to form, depends on the choice of the interaction kernel. Mogilner & Edelstein-Keshet (1999) showed that the type of kernel affects the possibility of movement and/or aggregation. Throughout the rest of this study,

we will consider translated Gaussian attraction and repulsion kernels (as in Eftimie *et al.* (2007); Carrillo de la Plata *et al.* (2015)):

$$K(x) = \frac{q_a}{\sqrt{2\pi m_a^2}} e^{-\frac{(x-s_a)^2}{2m_a^2}} - \frac{q_r}{\sqrt{2\pi m_r^2}} e^{-\frac{(x-s_r)^2}{2m_r^2}}, \quad (3.10)$$

where s_a and s_r represent half of the length of attraction and repulsion ranges, respectively, with $s_r < s_a$. Also, $m_j = s_j/8$, $j = a, r$, represent the width of the attractive and the repulsive interaction ranges. (The constants m_j , $j = a, r$, are chosen such that the support of more than 98% of the mass of the kernels is inside the interval $[0, \infty)$ (Eftimie *et al.*, 2007).) In Section 3.1 we will investigate how different types of kernels lead to different dispersion relations.

The Fourier sine transform of kernel (3.10) is given by

$$\hat{K}^s(k) = \int_{-\infty}^{\infty} K(r) \sin(kr) \, dr = q_a e^{-\frac{(km_a)^2}{2}} \sin(ks_a) - q_r e^{-\frac{(km_r)^2}{2}} \sin(ks_r). \quad (3.11)$$

Therefore, relation (3.9) becomes

$$-r_2 + \frac{2ks_2^*}{R} \left(1 + \tanh\left(a_2 \frac{p_2}{q}\right)\right) \left(q_a e^{-\frac{(km_a)^2}{2}} \sin(ks_a) - q_r e^{-\frac{(km_r)^2}{2}} \sin(ks_r)\right) > 0, \quad (3.12)$$

where the imaginary part of the eigenvalue $\lambda_3(k)$ will be zero.

An example of such dispersion relation is shown in Fig. 2. Note the steady-state/steady-state mode interaction that occurs when we increase the parameters q_a and q_r (i.e. the strength of attractive and repulsive cell–cell interactions). There is a range of k – values for which $Re(\lambda_3(k))$ is positive, and thus aggregations can arise from spatial perturbations of the steady state $(u_1^*, u_2^*, f^*, c^*) = (0, 1, 0, p_2/q)$. This means that the steady state $(0, 1, 0, p_2/q)$, which is linearly stable for the homogeneous system, is destabilized due to the spatial dynamics (diffusion and advection). Setting diffusion coefficient zero we observe that there is still a range of k – values for which $Re(\lambda_3(k)) > 0$, implying the adhesion-driven instability.

REMARK 3.1 Note that model (2.22) does not exhibit Hopf bifurcations (i.e. $Re(\lambda(k)) = 0, Im(\lambda(k)) \neq 0$). Therefore, although aggregations will develop, there will be no travelling patterns that arise via Hopf bifurcations.

3.1 Aggregation with different types of kernel

In Mogilner & Edelstein-Keshet (1999) it was shown that even kernels give rise to group drift, while odd kernels have a greater effect in regions where the distribution of the density is uneven (e.g. the edges of the population), leading to stationary groups. Considering the importance of the symmetry of the interaction kernels, we next discuss the cases of even and odd kernels, and compare these results with our previous results where we used a translated Gaussian kernel (see equation (3.10)), to investigate the possibility of cell aggregations to form from spatial perturbation of the steady state $(u_1^*, u_2^*, f^*, c^*) = (0, 1, 0, p_2/q)$.

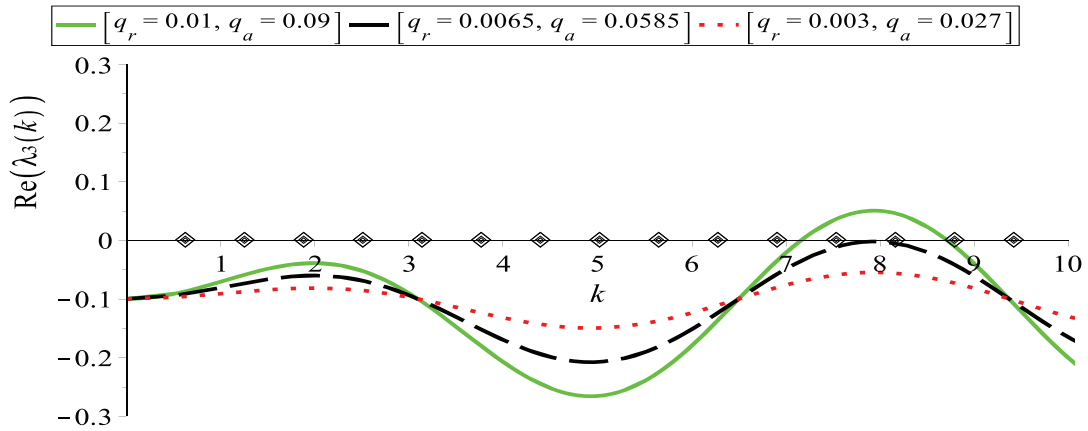


FIG. 2. Plot of the dispersion relation (3.12) for the steady state $(0, 1, 0, p_2/q)$. The curves represent $Re(\lambda_3(k))$ for: (a) $q_r = 0.01, q_a = 0.09$ (solid green curve); (b) $q_r = 0.0065, q_a = 0.0585$ (dashed black curve); (c) $q_r = 0.003, q_a = 0.027$ (dotted red curve); the rest of the model parameters are given in Table 2. The diamonds on the x-axis represent the discrete wave numbers $k_j = 2\pi j/L, j = 1, 2, \dots$. The two critical wave numbers that become unstable at the same time (giving rise to steady-state/steady-state mode interactions) are k_{12} and k_{13} .

- Aggregation with even kernel

We consider the situation that the interaction kernel is an even function with respect to the y-axis. We choose the following Gaussian kernel (Mogilner & Edelstein-Keshet, 1999):

$$K(x) := \frac{q_a}{\sqrt{2\pi m_a^2}} \exp\left(-x^2/2m_a^2\right) - \frac{q_r}{\sqrt{2\pi m_r^2}} \exp\left(-x^2/2m_r^2\right), \tag{3.13}$$

where q_a, q_r, m_a and m_r have the same meaning as in equation (3.10). The Fourier sine transform of the above even kernel is zero: $\hat{K}^s(k) = 0$. We know (see equation (3.8)) that the Jacobian matrix of system (3.6) has three negative eigenvalues $\lambda_{1,2,4} < 0$. For the even kernel considered here we also have

$$\lambda_3(k) = -r_2 < 0. \tag{3.14}$$

Therefore, the steady state $(u_1^*, u_2^*, f^*, c^*) = (0, 1, 0, p_2/q)$ is stable, and no aggregations will form.

- Aggregation with an odd kernel

We investigate now the stability of $(u_1^*, u_2^*, f^*, c^*) = (0, 1, 0, p_2/q)$ when we consider an odd kernel with respect to the origin. To this end, we choose

$$K(x) := \frac{q_a x}{\sqrt{2\pi m_a^2}} \exp\left(-x^2/2m_a^2\right) - \frac{q_r x}{\sqrt{2\pi m_r^2}} \exp\left(-x^2/2m_r^2\right), \tag{3.15}$$

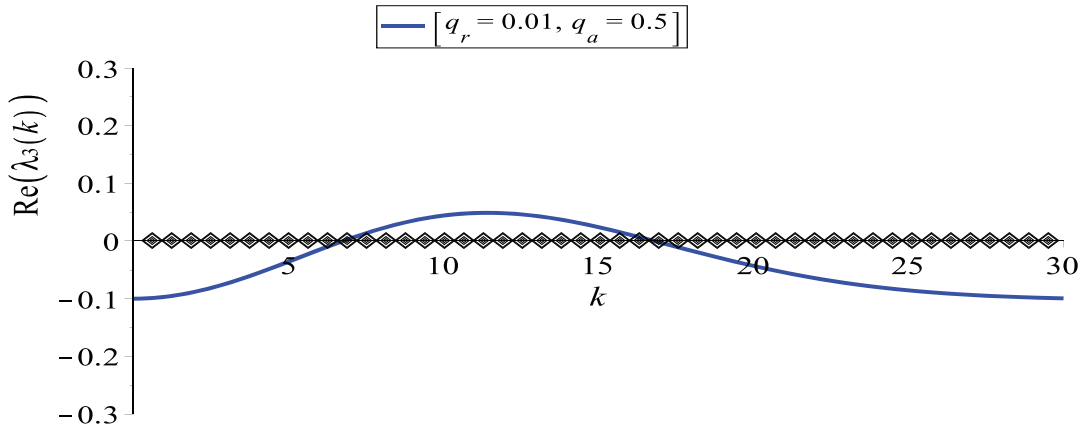


FIG. 3. Plot of the dispersion relation (3.17) for the steady state $(u_1^*, u_2^*, f^*, c^*) = (0, 1, 0, p_2/q)$. Here, $q_a = 0.5$. The rest of the model parameters are given in Table 2. The solid curve represents the real part of λ_3 , while the diamonds represent the discrete wave numbers $k_j = 2\pi \frac{j}{L}, j = 0, 1, 2, \dots$

where q_a, q_r, m_a and m_r have the same meaning as in equation (3.10). Then the Fourier sine transform of the kernel (3.15) is

$$\hat{K}^s(k) = q_a k m_a^2 \exp(-(k m_a)^2 / 2) - q_r k m_r^2 \exp(-(k m_r)^2 / 2). \tag{3.16}$$

As before, the Jacobian matrix of system (3.6) has three negative eigenvalues: $\lambda_{1,2,4} < 0$. The stability of the state $(0, 1, 0, p_2/q)$ is given by the sign of

$$\text{Re}(\lambda_3(k)) = -r_2 + \frac{2k^2 s_2^*}{R} \left(1 + \tanh\left(a_2 \frac{p_2}{q}\right) \right) \left(q_a m_a^2 e^{-\frac{(k m_a)^2}{2}} - q_r m_r^2 e^{-\frac{(k m_r)^2}{2}} \right). \tag{3.17}$$

In Fig. 3 we plot $\text{Re}(\lambda_3(k))$ against the wave number k for this steady state. We observe that for values of q_a greater than those in the translated Gaussian case (see Fig. 2), there is a range of k -values for which $\text{Re}(\lambda_3(k))$ is positive, thus the steady state $(0, 1, 0, p_2/q)$ can become unstable, and spatial aggregations could arise.

4. Numerical results

In this Section we investigate numerically the stability of model (2.22). To discretize our model we use a time-splitting approach. First, we use a Crank–Nicolson scheme to propagate the solution of the diffusion term. Then, we use the Nessyahu–Tadmor scheme (Nessyahu & Tadmor, 1990) for the time-propagation of the advection terms. Finally, for the time-propagation of the reaction terms we use a fourth order Runge–Kutta algorithm, where the integrals are further discretized using the Simpson’s rule. All simulations are performed on a domain of length $L = 10$ with periodic boundary conditions, and for time up to $t = 500$. Because of the periodic boundary conditions, we wrap the integrals around the

domain. The initial conditions for the cancer cell populations are either small random perturbations of spatially homogeneous steady states

$$\begin{aligned} u_i(x, 0) &= u_i^* + \text{rand}(0, 10^{-4}), \quad i = 1, 2, \\ f(x, 0) &= f^* + \text{rand}(0, 10^{-4}), \\ c(x, 0) &= c^* + \text{rand}(0, 10^{-4}), \end{aligned}$$

or small random perturbations of rectangular-shaped aggregations located in the middle of the domain

$$u_i(x, 0) = \begin{cases} u_i^c + \text{rand}(0, 10^{-4}), & x \in (L/2 - 1, L/2 + 1) \\ 0, & \text{everywhere else} \end{cases} \quad (4.1)$$

with $u_1^c = 0$ and u_2^c as specified in the caption of the figures. The initial conditions for the ECM and integrin density depend on cancer cell density, and are given by relations (2.17) and (2.18), for all numerical simulations.

STATIONARY AGGREGATION PATTERNS. To check the validity of our results obtained via linear stability analysis (see Fig. 2), we first run simulations for small random perturbations of the spatially homogeneous steady state $(u_1^*, u_2^*, f^*, c^*) = (0, 1, 0, p_2/q)$, and for $q_a = 0.09$ and $q_r = 0.01$. The results, presented in Fig. 4, show 12–13 stationary pulses (corresponding to critical wave numbers $k_{12} - k_{13}$). The spread of cancer cells over the whole domain (panels (a), (b)) leads to the degradation of ECM (panel (c)). The integrin density (panel (d)) follows the patterns in the density of cancer cells. We observe here a coexistence between a low u_1 population and a high u_2 population.

To check the effect of initial data on model dynamics, in Fig. 5 we investigate the behaviour of model (2.22) when we change the initial conditions to a rectangular pulse describing an initial aggregation of tumour cells. The magnitudes of attractive-repulsive interactions (and all other parameter values) are the same as in Fig. 4. The short-term results in Fig. 5(a)–(d) show a travelling pulse behaviour exhibited by the u_2 population that moves away from population u_1 (which is mostly stationary—although even this population spreads a bit). This faster spreading of the u_2 cells compared to the u_1 cells is consistent with experimental observations (Chapman *et al.*, 2014; Wojciechowska & Patton, 2015). The movement of u_2 population eventually stops near the boundary (due to the periodic boundary conditions, the left-moving and right-moving subgroups can sense each other across the boundary). The fast-moving u_2 cells degrade the ECM (panel (c)). We also note the high density of integrins associated with the u_1 population (panel (d)). The long-term results in Fig. 5(a')–(d') show the formation of new aggregations of cells at distant positions in space. For $t \in (100, 250)$, the two tumour populations coexist. For $t > 250$, population u_1 is slowly eliminated and population u_2 dominates the dynamics of model (2.22). We also note that despite some chaotic-like dynamics exhibited by the u_1 and u_2 populations for $t < 300$, in the long term the system approaches stationary pulses defined by 13 peaks (corresponding to unstable wave number k_{13}).

In Figs 6 and 7 we investigate the effect of various mutation rates on the dynamics of the u_1 and u_2 populations. In Fig. 6 we choose $M = 0.001$ (see Table 2), and observe that population u_2 vanishes for $t > 400$, while population u_1 persists and forms small high-density aggregations of cells. This unexpected behaviour might be explained by the combined effect of three factors: (i) the mutation rate ($M = 0.001$) that is much smaller than the growth rates ($r_{1,2} = 0.1$) of the two cancer cell populations,

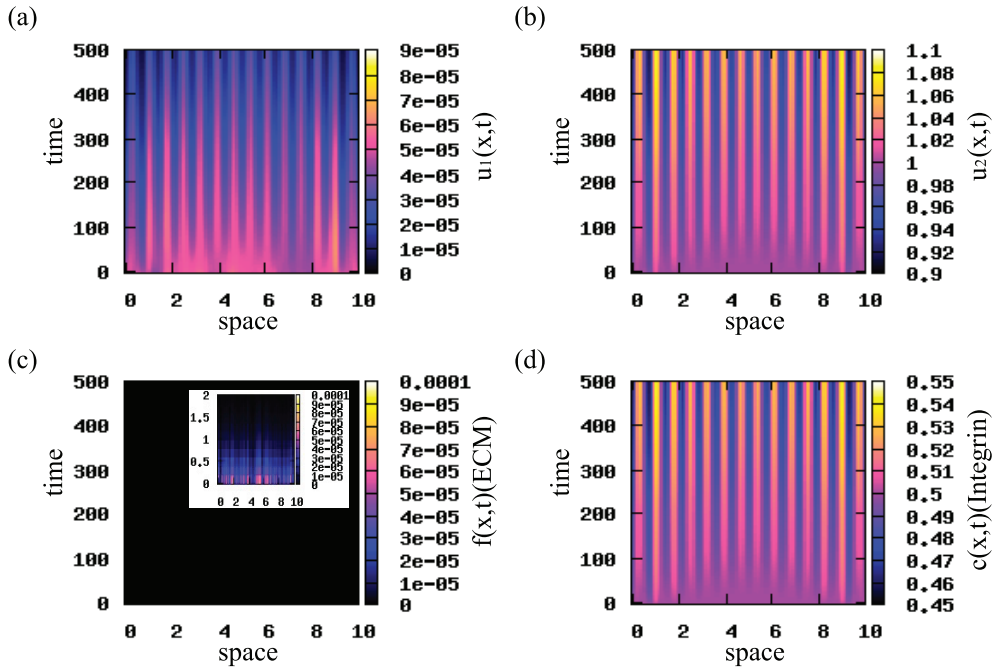


FIG. 4. Patterns exhibited by model (2.22) for small random perturbations of the steady state $(0, 1, 0, p_2/q)$, corresponding to the dispersion relation shown in Fig. 2. Here, we use the cell–cell interaction kernel given by relation (3.10), and the model parameters given in Table 2. (a) Density of u_1 cell population; (b) density of u_2 (highly mutated) cell population; (c) ECM density f ; (d) integrin density c . Note the formation of 12 or 13 peaks (if counting separately the peaks on the periodic boundaries) of high cell density corresponding to critical wave numbers k_{12}/k_{13} .

(ii) the lack of diffusion for u_2 and (iii) the competition for nutrients between the two cell populations (which is modelled implicitly by the logistic terms $G_{1,2}$; see equations (2.14)). This eventually leads to an overall increase in the first population, u_1 , and a decrease in the second (highly mutated) population, u_2 . In Fig. 7 we increase the mutation rate to $M = 0.05$, while choosing the growth rates fixed at $r_1 = r_2 = 0.1$. We observe that faster mutation rates lead to a decrease and eventual elimination of the u_1 population. The u_2 population increases and dominates the long-term dynamics of model (2.22).

TRAVELLING WAVE PATTERNS. Choosing again rectangular pulse initial conditions, we reduce the magnitudes of cell–cell attractive and repulsive interactions to $q_a = 0.00025$ and $q_r = 0.0005$. The numerical simulations in Fig. 8 show travelling waves that propagate in opposite directions at a constant speed. Similar behaviour is obtained for $q_a > q_r$. The evolution of the travelling waves is shown in Fig. 9 for $t = 25j$, $j = 1, \dots, 9$. We observe that the waves connect the unstable steady states $(0, 1, 0, p_2/q)$, with $p_2/q = 0.5$, and $(0, 0, f^*, 0)$, with $f^* = 1$.

Finally, we check the effect that an increase in the mutation rate M has on the travelling wave behaviour exhibited by model (2.22). Figure 10 shows that for high mutation rates ($M = 0.05$) the first population still exhibits a travelling wave before vanishing.

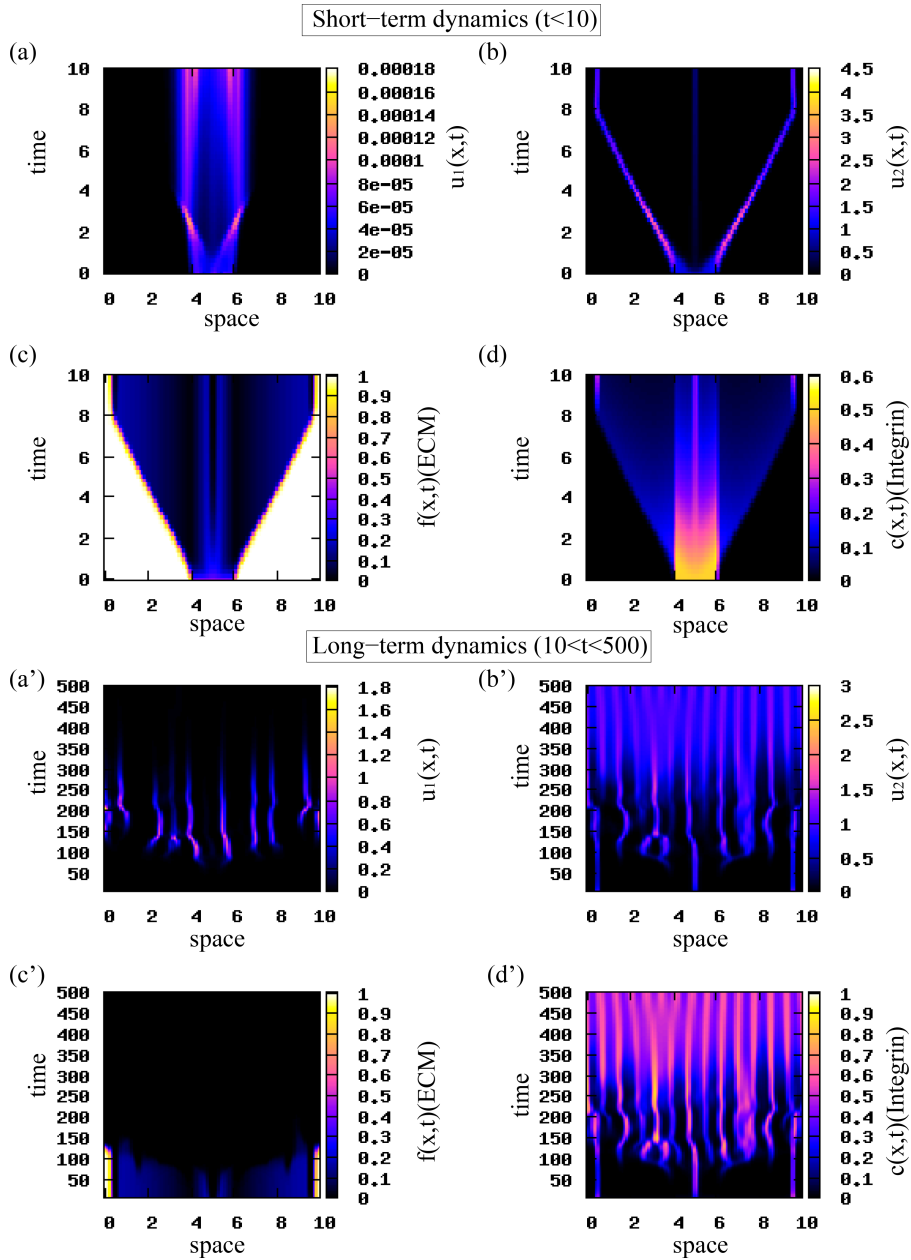


FIG. 5. Short-term and long-term patterns exhibited by model (2.22). The initial conditions for the two cancer cell populations are described by a rectangular pulse (see (4.1)) with $u_2^i = 1.0$. We use the interaction kernel given by (3.10), and the model parameters given in Table 2. (a),(a') Density of u_1 population; (b),(b') density of u_2 (highly mutated) population; (c),(c') ECM density f ; (d),(d') integrin density c .

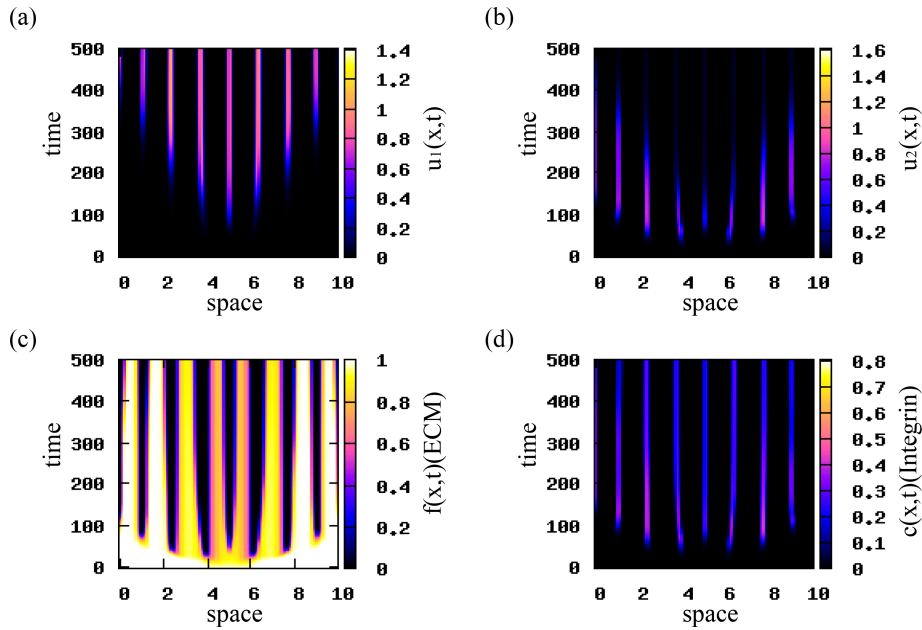


FIG. 6. Patterns exhibited by model (2.22). The initial conditions for the cancer cell populations consist of a rectangular pulse (see (4.1)) with $u_2^c = 0.001$. The mutation rate is $M = 0.001$. The rest of model parameters are given in Table 2. (a) Density of u_1 population; (b) density of u_2 population; (c) ECM density f ; (d) integrin density c .

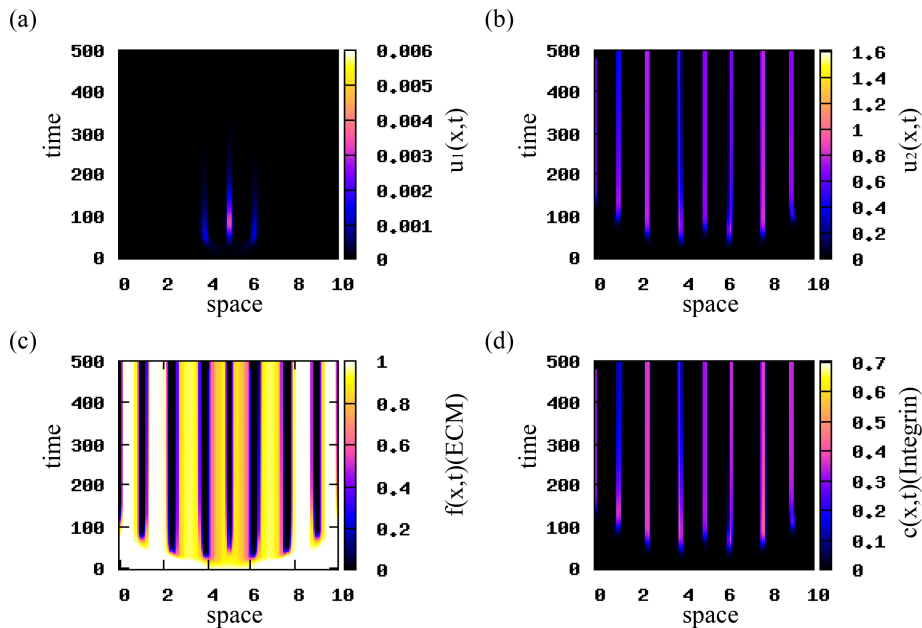


FIG. 7. Patterns exhibited by model (2.22). The initial conditions for the cancer cell populations consist of a rectangular pulse (see (4.1)) with $u_2^c = 0.001$. The mutation rate in $M = 0.05$. The rest of model parameters are given in Table 2. (a) Density of u_1 population; (b) density of u_2 population; (c) ECM density f ; (d) integrin density c .

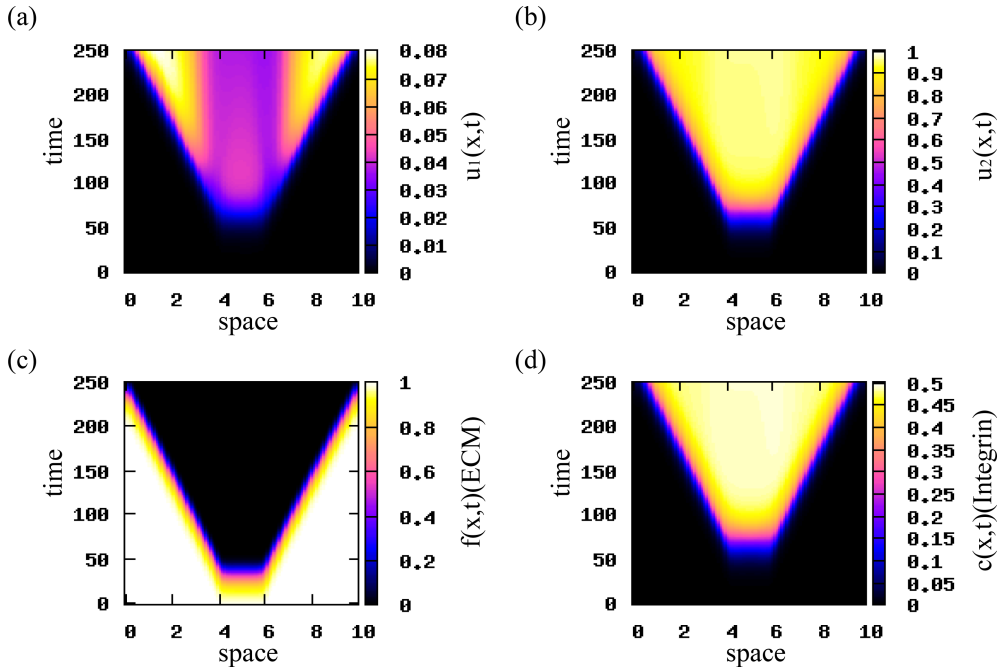


FIG. 8. Patterns exhibited by model (2.22) for initial conditions for the two cancer cell populations consisting of a rectangular pulse with $u_2^c = 0.001$. Here, $q_r = 0.0005$, $q_a = 0.00025$ and the rest of the model parameters are given in Table 2. (a) Cell density for u_1 population; (b) cell density for u_2 population; (c) ECM density f ; (d) integrin density c . Travelling waves are obtained for the translated Gaussian kernel given by relation (3.10).

REMARK 4.1 To understand the long-term behaviour of model (2.22) with odd kernels, we also ran numerical simulations using the interaction kernel given by (3.15). The spatial patterns obtained in this case were similar to the patterns obtained for the translated Gaussian kernel (see relation (3.10)).

4.1 Summary of model variables and parameters

Here we present two tables with the model variables and parameters. In Table 1 we list the model variables with their units. In Table 2 we list the parameters of our model and their corresponding units and non-dimensional values used in the simulations.

PARAMETER ESTIMATION.

- For the diffusion coefficient, [Chaplain & Lolas \(2006\)](#) has shown a range between $\tilde{D} = 10^{-5}$ and $\tilde{D} = 10^{-3}$. In this study, we choose $\tilde{D} = 10^{-4}$.
- The sensing radius was based on the range of values given in ([Armstrong et al., 2006](#); [Gerisch & Chaplain, 2008](#)). In this study, we choose $\tilde{R} = 0.99$.
- Attraction and repulsion ranges were chosen to be smaller or equal to sensing radius, with the repulsion range to be smaller than the attraction range ([Green et al., 2010](#)).

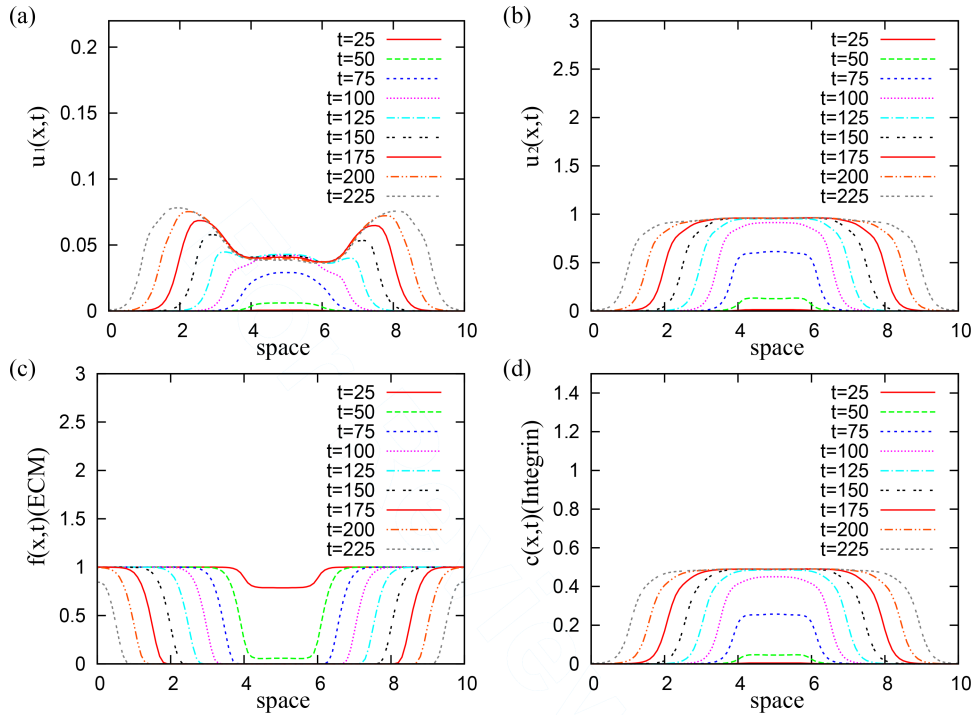


FIG. 9. The evolution of the travelling waves under small perturbations for $q_r = 0.0005$, $q_a = 0.00025$ and the rest of the model parameters given in Table 2, of (a) cancer cell density u_1 of the first ('normal') population; (b) cancer cell density u_2 of the second ('mutant') population; (c) ECM density f ; (d) integrin density c .

- Various experimental studies (Cunningham & You, 2015; Morani *et al.*, 2014) have shown that doubling times for tumour cells range from 1–10 days. This corresponds to growth rates between $(\ln(2)/10, \ln(2)/1) = (0.07, 0.7)$. In this study, we assume that $\tilde{r}_1 = \tilde{r}_2 = 0.1$.
- Experimental studies (Cillo *et al.*, 1987; Hill *et al.*, 1984; Mareel *et al.*, 1991) have shown that the mutation rate ranges between $M = 10^{-3}/\text{day}$ and $M = 0.1/\text{day}$. Thus the non-dimensional value of the mutation rate is in the range between $\tilde{M} = 0.001$ and $\tilde{M} = 0.1$ (for highly aggressive tumours). In this study, we choose $\tilde{M} = 0.001$.
- The parameters $a_i, d, b_i, s_i^*, s^*, c_i^*, i = 1, 2$, were based on the range of the adhesion strength parameters used in Armstrong *et al.* (2006).
- Experimental studies (Kidera *et al.*, 2010) have shown greater production of integrins for highly mutated cancer cells. Thus, we choose $\tilde{p}_1 < \tilde{p}_2$.
- Experimental studies (Delcommenne & Streuli, 1995; Davis *et al.*, 2001; Liu *et al.*, 2011; Lobert *et al.*, 2010) have shown that the half-lives of the integrins range from 0.04–4 days. This corresponds to decay rate between $(\ln(2)/4, \ln(2)/0.04) = (0.17, 17.3)$. In this study, we assume that $\tilde{q} = 0.2$.

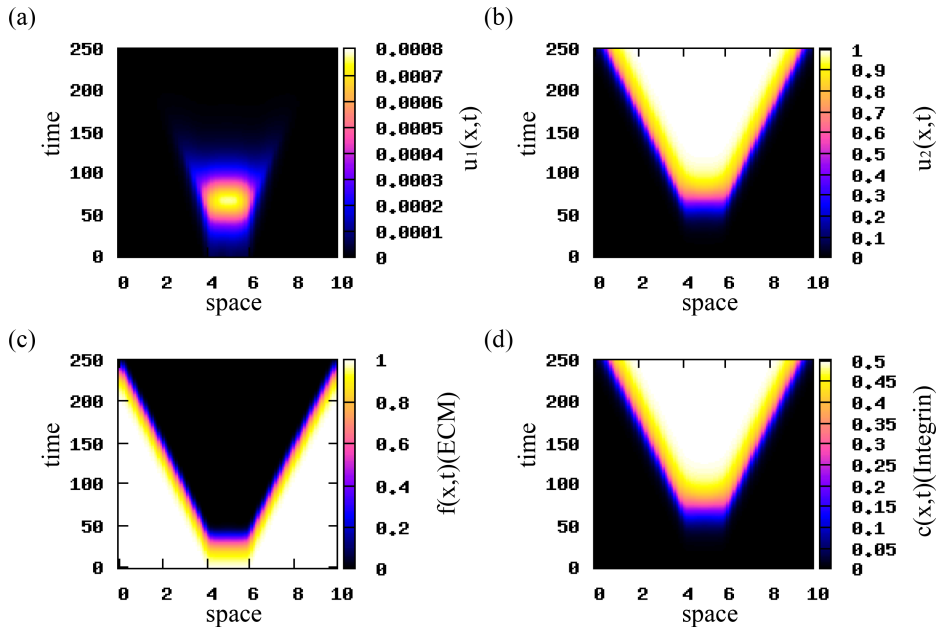


FIG. 10. Patterns exhibited by model (2.22) for higher mutation rates ($M = 0.05$) and initial conditions for the two cancer cell populations consisting of a rectangular pulse with $u_2^c = 0.001$. Here, $q_r = 0.0005$, $q_a = 0.00025$ and the rest of the model parameters are given in Table 2. (a) Cell density for u_1 population; (b) cell density for u_2 population; (c) ECM density f ; (d) integrin density c . Travelling waves are obtained for the translated Gaussian kernel given by relation (3.10)

5. Speed of travelling waves

The numerical simulations showed that the model exhibits travelling wave solutions (see Figs 8 and 9). In this section we estimate the minimum speed at which these waves could propagate (assuming that the travelling waves do exist). We assume that close to the invading front, the nonlinear differential equations describing the spread of a population have similar speeds as their linear approximation (see the approaches in Medlock & Kot (2003); Mollison (1991)). Therefore, we first calculate the linearized system (3.5) at the steady state $(u_1^*, u_2^*, f^*, c^*) = (0, 1, 0, p_2/q)$. In travelling wave coordinates $z = x - wt$ (where $u_i(x, t) = U_i(z)$, $i = 1, 2$, $f(x, t) = F(z)$, $c(x, t) = C(z)$), this system becomes:

$$-wU_1'(z) = DU_1''(z) - MU_1(z), \tag{5.1a}$$

$$-wU_2'(z) = -\frac{1}{R} \frac{\partial}{\partial z} \left\{ \int_0^R K(r) [S_2(p_2/q)(U_2(z+r) - U_2(z-r)) + S(p_2/q)(U_1(z+r) - U_1(z-r)) + C_2(p_2/q)(F(z+r) - F(z-r))] dr \right\} + MU_1(z) - r_2(U_1(z) + U_2(z)), \tag{5.1b}$$

$$-wF'(z) = -\beta F(z), \quad (5.1c)$$

$$-wC'(z) = p_1 U_1(z) + p_2 U_2(z) - qC(z). \quad (5.1d)$$

Let $s_1, s_2, s_3, s_4 > 0$ be the steepness (i.e. exponent of an exponential decay/increase profile) of u_1, u_2, f, c . The minimum of $w(s_j)$ for $s_j > 0, j = 1, \dots, 4$, gives an upper bound on the rightward travelling wave speed of the nonlinear system. Thus, we make the general exponential ansatz

$$U_1(z) = A_1 e^{-s_1 z}, U_2(z) = A_2 e^{-s_2 z}, F(z) = A_3 e^{s_3 z} \text{ and } C(z) = A_4 e^{-s_4 z}, \quad (5.2)$$

where $A_j \in \mathbb{R}, j = 1, \dots, 4$, such that asymptotically we have $U_i(z) \rightarrow 0, i = 1, 2, F(z) \rightarrow f^*, C(z) \rightarrow 0$ as $z \rightarrow +\infty$. First we investigate the $s_j, j = 1, \dots, 4$, numerically. In Fig. 11 we fit these exponential ansatz profiles (given by (5.2)) to the numerical solutions $u_1(x, t), u_2(x, t), f(x, t)$ and $c(x, t)$ at time $t = 175$ (dotted curve). We obtain the following ansatz profiles (continuous curve in Fig. 11):

$$E_1(x) = A_1 \cdot \exp(-3.17x), \text{ with } A_1 = 0.063 \cdot \exp(24.5675), \quad (5.3)$$

$$E_2(x) = A_2 \cdot \exp(-3.17x), \text{ with } A_2 = 0.8 \cdot \exp(24.2505), \quad (5.4)$$

$$E_3(x) = A_3 \cdot \exp(6x), \text{ with } A_3 = 0.82 \cdot \exp(-52.5), \quad (5.5)$$

$$E_4(x) = A_4 \cdot \exp(-3.17x), \text{ with } A_4 = 0.4 \cdot \exp(24.092). \quad (5.6)$$

Hence, we deduce that the travelling wave profiles of $U_1(z), U_2(z)$ and $C(z)$ have the same steepness $s := s_1 = s_2 = s_4 = 3.17$, while the profile of $F(z)$ has steepness $s_3 = 6$. Therefore, we replace the exponential ansatz given by (5.2) with $U_1(z) = A_1 e^{-sz}, U_2(z) = A_2 e^{-sz}, F(z) = A_3 e^{s_3 z}$ and $C(z) = A_4 e^{-sz}$. Let us assume that $K(r)$ has a moment generating function, $\tilde{M}(s)$, defined as

TABLE 1 A list of model variables with their units. Since we are in 1D, length and volume coincide and we express the variables in terms of domain length.

Variable	Description	Dimensional Units
u_1	'Normal' cancer cell density	cell/length
u_2	'Mutant' cancer cell density	cell/length
f	ECM density	mg/length
c	Integrin density	integrins/cell

TABLE 2 A list of model parameters with their units and their non-dimensional values, obtained from (2.20) and (2.21), which we used during numerical simulations.

Param.	Description	Dimensional Units	Non-dim. value (\tilde{p})	Reference
D	Diffusion coefficient	$length^2/time$	10^{-4}	Chaplain & Lolas (2006)
R	Sensing radius	$length$	0.99	Armstrong <i>et al.</i> (2006)
q_a	Magnitude of attraction	$length^2/cell$	0.09	Estimated
q_r	Magnitude of repulsion	$length^2/cell$	0.01	Estimated
s_a	Attraction range	$length$	0.99	Estimated
s_r	Repulsion range	$length$	0.25	Estimated
m_a	Width of attraction kernel	$length$	0.99/8	Estimated
m_r	Width of repulsion kernel	$length$	0.25/8	Estimated
r_1	Growth rate of u_1	$1/time$	0.1	Cunningham & You (2015); Morani <i>et al.</i> (2014)
r_2	Growth rate of u_2	$1/time$	0.1	Cunningham & You (2015); Morani <i>et al.</i> (2014)
M	Mutation rate	$1/time$	0.001	Cillo <i>et al.</i> (1987); Hill <i>et al.</i> (1984); Mareel <i>et al.</i> (1991)
a_1	Coeff. related to the number of integrins necessary for max self-adhesion between u_1	$cell/integrins$	0.3	Estimated
a_2	Coeff. related to the number of integrins necessary for max self-adhesion between u_2	$cell/integrins$	0.01	Estimated
d	Coeff. related to the number of integrins necessary for max cross-adhesion	$cell/integrins$	0.5	Estimated
b_1	Coeff. related to the number of integrins necessary for max cell-ECM adhesion for u_1	$cell/integrins$	1.8	Estimated
b_2	Coeff. related to the number of integrins necessary for max cell-ECM adhesion for u_2	$cell/integrins$	5	Estimated
s_1^*	Magnitude of self-adhesion forces of u_1	$length/(time \cdot cell)$	0.9	Estimated
s_2^*	Magnitude of self-adhesion forces of u_2	$length/(time \cdot cell)$	0.2	Estimated
s^*	Magnitude of cross-adhesion forces	$length/(time \cdot cell)$	1	Estimated

(continued).

TABLE 2 *Continued.*

Param.	Description	Dimensional Units	Non-dim. value (\tilde{p})	Reference
c_1^*	Magnitude of cell-ECM forces of u_1	$length / (time \cdot cell)$	1.5	Estimated
c_2^*	Magnitude of cell-ECM forces of u_2	$length / (time \cdot cell)$	5.5	Estimated
α	Rate of ECM degradation by u_1	$length / (time \cdot cell)$	1	Sherratt <i>et al.</i> (2009)
β	Rate of ECM degradation by u_2	$length / (time \cdot cell)$	2	Sherratt <i>et al.</i> (2009)
p_1	Production rate of c by u_1	$integrins / (time \cdot cell)$	0.05	Estimated
p_2	Production rate of c by u_2	$integrins / (time \cdot cell)$	0.1	Estimated
q	Decay rate of c	$1/time$	0.2	Liu <i>et al.</i> (2011)

$\tilde{M}(s) := \int_{-\infty}^{+\infty} K(r) (e^{-sr} - e^{sr}) dr$ (and such a function exists for the translated Gaussian kernels (3.10)). Then we obtain from system (5.1):

$$A_1 (sw - s^2D + M) = 0, \quad (5.7a)$$

$$A_1 \left(-S(p_2/q) \frac{s\tilde{M}(s)}{R} - M + r_2 \right) + A_2 \left(sw - S_2(p_2/q) \frac{s\tilde{M}(s)}{R} + r_2 \right) + A_3 e^{(s+s_3)z} \left(-C_2(p_2/q) \frac{s_3\tilde{M}(s_3)}{R} \right) = 0, \quad (5.7b)$$

$$A_3 (s_3w - \beta) = 0, \quad (5.7c)$$

$$-A_1p_1 - A_2p_2 + A_4 (sw + q) = 0. \quad (5.7d)$$

Taking now the determinant of the system equal to zero we have the characteristic relation

$$(sw - s^2D + M) \left(sw - S_2(p_2/q) \frac{s\tilde{M}(s)}{R} + r_2 \right) (s_3w - \beta) (sw + q) = 0. \quad (5.8)$$

Since we are looking for the minimum positive speed with respect to $s > 0$ and $s_3 > 0$, in Fig. 12(a) we plot implicitly equation (5.8) in the (s, w) -space. Note that the steepness coefficient s_3 (for the ECM degradation profile) does not have any significant effect on the minimum positive wave speed w (of the invading u_1 and u_2 populations). For this reason, in Fig. 12(b) we plot the relation (5.8) in the (s, w) -plane for fixed $s_3 > 0$. We see that indeed we cannot have a travelling wave with positive speed unless the wave has a steepness $s > 3.17$. Moreover, faster waves have higher steepness.

Finally, we are interested in investigating how the speed of the invading waves correlates with their steepness, as we vary different model parameters. In Fig. 13(a) we see that a decrease in the diffusion coefficient D by one order of magnitude leads to a reduction in the velocity $w > 0$. In Fig. 13(b) we see that an increase in the mutation rate M (from 0.001 to 0.05) leads to a slightly lower velocity $w > 0$ and

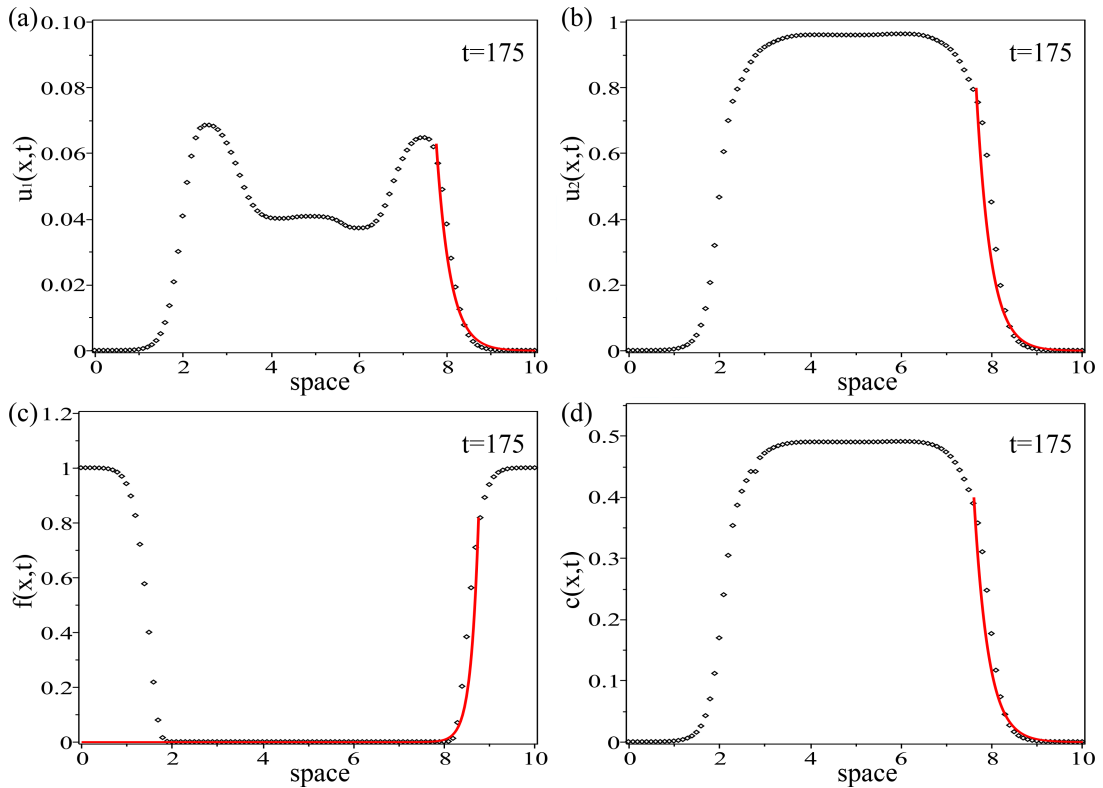


FIG. 11. Plot of the numerical simulations of the travelling wave profile, shown in Figs 8 and 9, for (a) population u_1 and the exponential ansatz function $E_1(x)$ given by relation (5.3) with $A_1 = 0.063 \cdot \exp(24.5675)$; (b) population u_2 and the exponential ansatz function $E_2(x)$ given by relation (5.4) with $A_2 = 0.8 \cdot \exp(24.2505)$; (c) ECM density, f , and the exponential ansatz function $E_3(x)$ given by relation (5.5) with $A_3 = 0.82 \cdot \exp(-52.5)$; (d) integrin density, c , and the exponential ansatz function $E_4(x)$ given by relation (5.6) with $A_4 = 0.4 \cdot \exp(24.092)$. Here, $q_r = 0.0005$, $q_a = 0.00025$ and the rest of the model parameters are given in Table 2.

a higher steepness. (Note that for $s > 100$, the invading speed obtained for $M = 0.001$ and $M = 0.05$ is the same—not shown here.)

6. Conclusions and discussion

In this paper we introduced a model of integro-differential equations describing the dynamics of two cancer cell populations: a ‘normal’ cell population that exhibits both random and directed movement, and a ‘mutant’ cell population that exhibits only directed movement. The model incorporated both nonlocal cell–cell interactions and cell–matrix interactions. Moreover, unlike other models in the literature, in our model these interactions were not constant but depended on the cellular level of integrins.

Linear stability analysis of the non-dimensional model showed that aggregations could arise only via real bifurcations (the system could not exhibit Hopf bifurcations). Numerical results showed that these aggregations were described by a large number of stationary pulses (e.g. 13 pulses corresponding to the

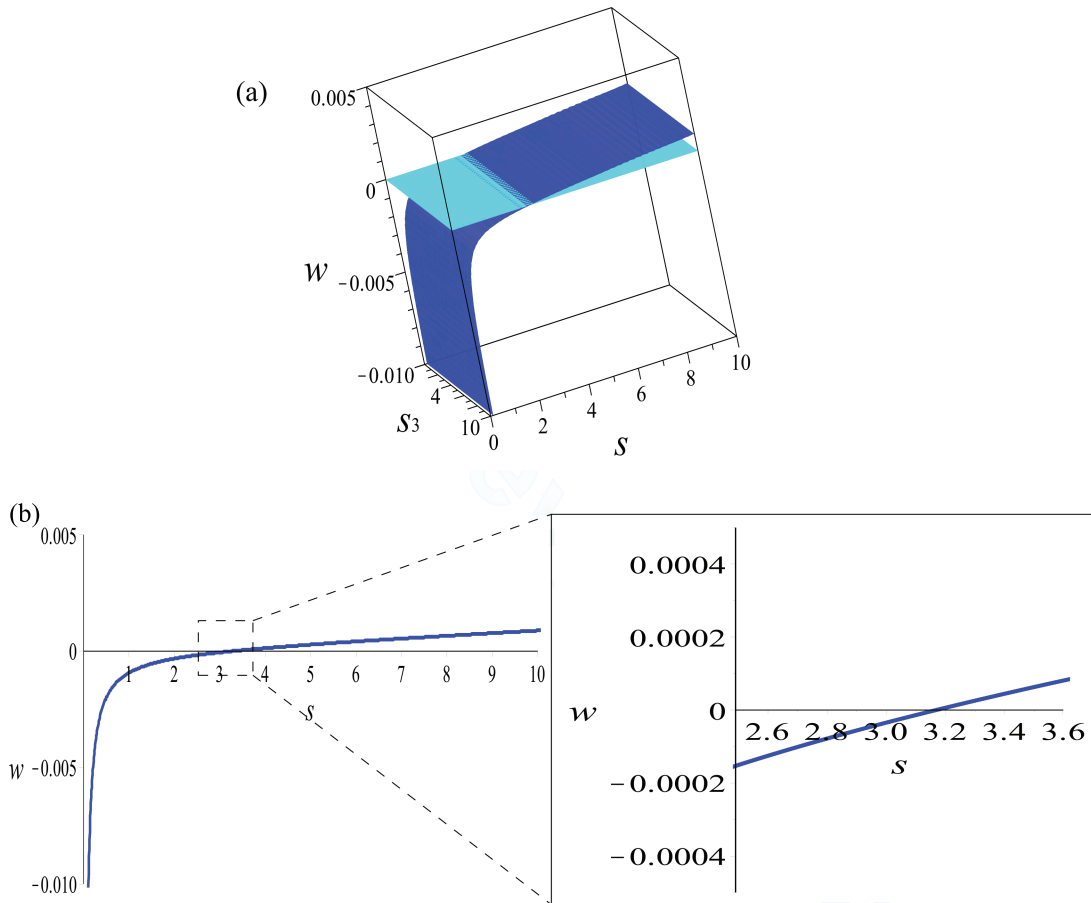


FIG. 12. Plot of the relation (5.8) for $q_r = 0.0005$, $q_a = 0.00025$ and the rest of the model parameters as given in Table 2. The plot shows the relation between the speed and the steepness of the travelling waves in the (a) (s, s_3, w) -space; (b) (s, w) -plane.

critical unstable wave number k_{13}). Moreover, numerics also showed the existence of travelling waves. We investigated the speed of these waves, which seemed to be affected by the diffusion coefficient and the mutation rate of cells.

The rate at which cancer cells mutate seemed to play a critical role in our model. In Figs 6 and 7 (as well as Figs 8 and 10) we showed that depending on the magnitude of the mutation rate, either the u_1 or the u_2 cell populations can be eliminated (or, in some cases they can co-exist—see Figs 4 and 8). The existence of these dominant behaviours exhibited by the u_1 or u_2 populations are consistent with the principle of competitive exclusion of clonal sub-populations in heterogeneous tumours (Egan *et al.*, 2012; Keats *et al.*, 2012; Leith *et al.*, 1989). In Fisher *et al.* (2013) the authors interpreted the experimental data, which showed suppression and reappearance of cancer clones in myeloma patients (Keats *et al.*, 2012) and chronic lymphocytic leukaemia patients (Schuh *et al.*, 2012), by suggesting that two subclones can exist in a dynamic equilibrium. While all these experimental studies record the survival/suppression of tumour clones in various cancers, they do not offer a mechanistic explanation

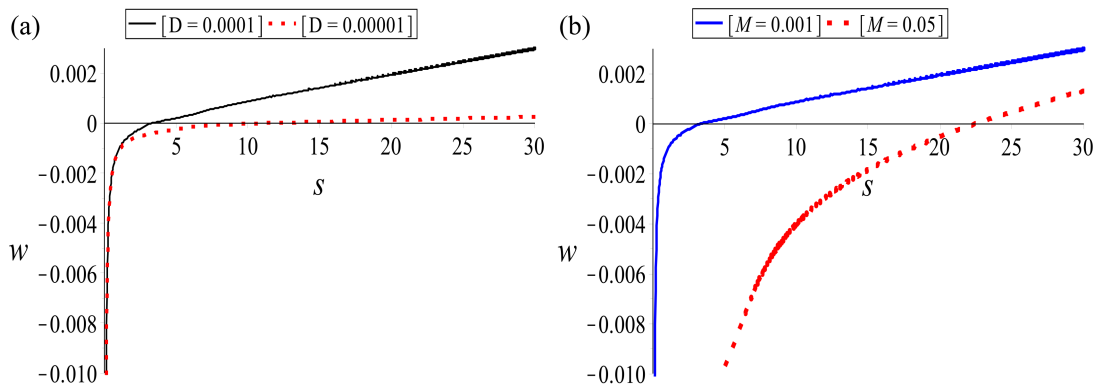


FIG. 13. Plot of the relation (5.8) for $q_r = 0.0005$, $q_a = 0.00025$, and the rest of the model parameters as given in Table 2, as we vary: (a) diffusion coefficient D : $D = 10^{-4}$ (black solid curve) and $D = 10^{-5}$ (red dashed curve); (b) mutation rate M : $M = 0.001$ (blue solid curve) and $M = 0.05$ (red dashed curve).

for the factors that could lead to these behaviours. In contrast, our numerical results (see Figs 6 and 7, 8 and 10) offer such a mechanistic explanation by identifying the magnitude of the mutation rate as a factor that could explain the experimentally observed suppression and reappearance of cancer clones.

This issue of cancer heterogeneity has significant implications on cancer drug therapies, since it can lead to drug resistance. For example, clinical studies have shown the emergence of imatinib-resistant mutation clones in patients with chronic myeloid leukaemia, which can co-exist with subclones that carry different imatinib-resistant mutations in treatment-naïve patients (Shah *et al.*, 2002). Overall, these clinical observations suggest that a single drug might not be successful in treating a genetically heterogeneous tumour, since sub-populations of cancer cells with drug-resistant mutations could become dominant, thus leading to therapeutic failure.

We note that the spatial distribution of the two cancer sub-populations, with the original u_1 population in the centre of the aggregation and the mutated u_2 clones towards the edges of the aggregation (see Fig. 5 for $t \in [0, 10]$ or Fig. 6 for $t \in [100, 300]$), is consistent with experimental studies on the spatial relationship between clonal sub-populations of hepatocellular carcinoma (HCC) tumour (Ling *et al.*, 2015). In this experimental study, the authors investigated the clonal diversity of a HCC-15 tumour (and the spatial distribution of these clones), and showed the ancestral clones being positioned in the middle of the tumour, with the descendant clones radiating outward.

The numerical results of the model presented in this paper show that cell–cell/cell–matrix adhesion combined with cell proliferation (in the presence of cell competition) and cell mutation, can impact which tumour clones survive (see Figs 4–8 and 10). Therefore, our model puts forward the idea that in order to predict the emergence of a particular cancer clone, we should first quantify cell–cell and cell–matrix adhesive interactions for the various tumour clones, and their proliferative capacities.

In this paper we focused on a 1D model. However, real life cell dynamics occurs in 2D or 3D. In Appendix A we extended model (2.22) to two spatial dimensions. Moreover, to verify if the linear stability results for the 1D model (2.22) were valid also in 2D, we applied linear stability analysis. We showed that for similar kernels, we obtained similar dispersion relations with no imaginary parts (and hence no Hopf bifurcations). Therefore, we expect that the 2D model (A1) would exhibit stationary pulses similar to the ones exhibited by the 1D model (2.22). Future work will consider extending the numerical results in 2D.

Acknowledgements

V. B. acknowledges support from an Engineering and Physical Sciences Research Council (UK) grant number EP/L504932/1. R. E. acknowledges support from an Engineering and Physical Sciences Research Council (UK) grant number EP/K033689/1.

REFERENCES

- AABO, K., VINDELØV, L. & SPANG-THOMSEN, M. (1994) Interaction between three subpopulations of Ehrlich carcinoma in mixed solid tumours in nude mice: evidence of contact domination. *Brit. J. Cancer*, **70**, 91–96.
- AMBROSI, D. & PREZIOSI, L. (2002) On the closure of mass balance models for tumor growth. *Math. Models Methods Appl. Sci.*, **12**, 737–754.
- ANDASARI, V., GERISCH, A., LOLAS, G., SOUTH, A. P. & CHAPLAIN, M. A. J. (2011) Mathematical modeling of cancer cell invasion of tissue: biological insight from mathematical analysis and computational simulation. *J. Math. Biol.*, **63**, 141–171.
- ANDASARI, V. & CHAPLAIN, M. A. J. (2012) Intracellular modelling of cell-matrix adhesion during cancer cell invasion. *Math. Model. Nat. Phenom.*, **7**, 29–48.
- ANDERSON, A. R. A., CHAPLAIN, M. A. J., NEWMAN, E. L., STEELE, R. J. C. & THOMPSON, A. M. (2000) Mathematical modelling of tumour invasion and metastasis. *J. Theor. Med.*, **2**, 129–154.
- ARMSTRONG, N. J., PAINTER, K. J. & SHERRATT, J. A. (2006) A continuum approach to modelling cell-cell adhesion. *J. Theor. Biol.*, **243**, 98–113.
- BECKMANN, M. W., NIEDERACHER, D., SCHNÜRCH, H.-G., GUSTERSON, B. A. & BENDER, H. G. (1997) Multistep carcinogenesis of breast cancer and tumour heterogeneity. *J. Mol. Med.*, **75**, 429–439.
- BELLOMO, N., BELLOUQUID, A., NIETO, J. & SOLER, J. (2010) Complexity and mathematical tools toward the modelling of multicellular growing systems. *Math. Comput. Model.*, **51**, 441–451.
- BENEDETTO, S., PULITO, R., CRICH, S. G., TARONE, G., AIME, S., SILENGO, L. & HAMM, J. (2006) Quantification of the expression level of integrin receptor $\alpha v \beta 3$ in cell lines and MR imaging with antibody-coated iron oxide particles. *Magn. Reson. Med.*, **56**, 711–716.
- BENSON, D. L., SHERRATT, J. A. & MAINI, P. K. (1993) Diffusion driven instability in an inhomogeneous domain. *Bull. Math. Biol.*, **55**, 365–384.
- BITSOUNI, V., CHAPLAIN, M. A. J. & EFTIMIE, R. (2017) Mathematical modelling of cancer invasion: the multiple roles of TGF- β pathway on tumour proliferation and cell adhesion. *Math. Models Methods Appl. Sci.*, **27**, 1929–1962.
- BYRNE, H. & CHAPLAIN, M. (1996) Modelling the role of cell–cell adhesion in the growth and development of carcinomas. *Math. Comput. Model.*, **24**, 1–17.
- BYRNE, H. & PREZIOSI, L. (2003) Modelling solid tumour growth using the theory of mixtures. *Math. Med. Biol.*, **20**, 341–366.
- CALVO, F. & SAHAI, E. (2011) Cell communication networks in cancer invasion. *Curr. Opin. Cell Biol.*, **23**, 621–629.
- CARRILLO DE LA PLATA, J. A., EFTIMIE, R. & HOFFMANN, F. (2015) Non-local kinetic and macroscopic models for self-organised animal aggregations. *Kinetic Relat. Models*, **8**, 413–441.
- CHAPLAIN, M. A. J., LACHOWICZ, M., SZYMAŃSKA, Z. & WRZOSEK, D. (2011) Mathematical modelling of cancer invasion: the importance of cell–cell adhesion and cell–matrix adhesion. *Math. Models Methods Appl. Sci.*, **21**, 719–743.
- CHAPLAIN, M. A. J. & LOLAS, G. (2006) Mathematical modelling of cancer invasion of tissue: dynamic heterogeneity. *Netw. Heterog. Media*, **1**, 399–439.
- CHAPMAN, A., DEL AMA, L. F., FERGUSON, J., KAMARASHEV, J., WELLBROCK, C. & HURLSTONE, A. (2014) Heterogeneous tumor subpopulations cooperate to drive invasion. *Cell Rep.*, **8**, 688–695.
- CILLO, C., DICK, J. E., LING, V. & HILL, R. P. (1987) Generation of drug-resistant variants in metastatic B16 mouse melanoma cell lines. *Cancer Res.*, **47**, 2604–2608.

- CRISTINI, V., LI, X., LOWENGRUB, J. S. & WISE, S. M. (2009) Nonlinear simulations of solid tumor growth using a mixture model: invasion and branching. *J. Math. Biol.*, **58**, 723–763.
- CUNNINGHAM, D. & YOU, Z. (2015) In vitro and in vivo model systems used in prostate cancer research. *J. Biol. Meth.*, **2**, e17.
- CUTLER, S. M. & GARCÍA, A. J. (2003) Engineering cell adhesive surfaces that direct integrin $\alpha_5\beta_1$ binding using a recombinant fragment of fibronectin. *Biomaterials*, **24**, 1759–1770.
- DAVIS, T. L., RABINOVITZ, I., FUTSCHER, B. W., SCHNÖLZER, M., BURGER, F., LIU, Y., KULESZ-MARTIN, M. & CRESS, A. E. (2001) Identification of a novel structural variant of the α_6 integrin. *J. Biol. Chem.*, **276**, 26099–26106.
- DEAKIN, N. E. & CHAPLAIN, M. A. J. (2013) Mathematical modeling of cancer invasion: the role of membrane-bound matrix metalloproteinases. *Front. Oncol.*, **3**, 70.
- DELCOMMENNE, M. & STREULI, C. H. (1995) Control of integrin expression by extracellular matrix. *J. Biol. Chem.*, **270**, 26794–26801.
- DEMAN, J. J., VAKAET, L. C. & BRUYNEEL, E. A. (1976) Cell size and mutual cell adhesion. II. Evidence for a relation between cell size, long-range electrostatic repulsion and intercellular adhesiveness during density-regulated growth in suspension. *J. Membr. Biol.*, **26**, 205–215.
- DOMSCHKE, P., TRUCU, D., GERISCH, A. & CHAPLAIN, M. A. J. (2014) Mathematical modelling of cancer invasion: implications of cell adhesion variability for tumour infiltrative growth patterns. *J. Theor. Biol.*, **361**, 41–60.
- DOMSCHKE, P., TRUCU, D., GERISCH, A. & CHAPLAIN, M. (2017) Structured models of cell migration incorporating molecular binding processes. *J. Math. Biol.*, **75**, 1517–1561.
- DYSON, R., GREEN, J., WHITELEY, J. & BYRNE, H. (2016) An investigation of the influence of extracellular matrix anisotropy and cell-matrix interactions on tissue architecture. *J. Math. Biol.*, **72**, 1775–1809.
- EDELSTEIN-KESHET, L. & ERMENTROUT, G. (1990) Models for contact-mediated pattern formation: cells that form parallel arrays. *J. Theor. Biol.*, **29**, 33–58.
- EFTIMIE, R., DE VRIES, G., LEWIS, M. A. & LUTSCHER, F. (2007) Modeling group formation and activity patterns in self-organizing collectives of individuals. *Bull. Math. Biol.*, **69**, 1537–1565.
- EGAN, J. B., SHI, C.-X., TEMBE, W., CHRISTOFORIDES, A., KURDOGLU, A., SINARI, S., MIDDHA, S., ASMANN, Y., SCHMIDT, J., BRAGGIO, E. *et al.* (2012) Whole-genome sequencing of multiple myeloma from diagnosis to plasma cell leukemia reveals genomic initiating events, evolution, and clonal tides. *Blood*, **120**, 1060–1066.
- ENDERLING, H., ANDERSON, A. R., CHAPLAIN, M. A. J., MUNRO, A. J. & VAIDYA, J. S. (2006) Mathematical modelling of radiotherapy strategies for early breast cancer. *J. Theor. Biol.*, **241**, 158–171.
- ENDERLING, H., CHAPLAIN, M. A. J. & HAHNFELDT, P. (2010) Quantitative modeling of tumor dynamics and radiotherapy. *Acta Biotheor.*, **58**, 341–353.
- ENGWER, C., HILLEN, T., KNAPPITSCH, M. & SURULESCU, C. (2015) Glioma follow white matter tracts: a multiscale dti-based model. *J. Math. Biol.*, **71**, 551–582.
- ENGWER, C., STINNER, C. & SURULESCU, C. (2017) On a structured multiscale model for acid-mediated tumor invasion: the effects of adhesion and proliferation. *Math. Models Methods Appl. Sci.*, **27**, 1355.
- ERBAN, R. & OTHMER, H. (2004) From individual to collective behaviour in bacterial chemotaxis. *SIAM J. Appl. Math.*, **65**, 362–394.
- ERBAN, R. & OTHMER, H. (2005) From signal transduction to spatial pattern formation in *e. coli*: a paradigm for multiscale modeling in biology. *Multiscale Model. Simul.*, **3**, 362–394.
- FETECAU, R. C. (2011) Collective behavior of biological aggregations in two dimensions: a nonlocal kinetic model. *Math. Models Methods Appl. Sci.*, **21**, 1539–1569.
- FETECAU, R. C. & EFTIMIE, R. (2010) An investigation of a nonlocal hyperbolic model for self-organization of biological groups. *J. Math. Biol.*, **61**, 545–579.
- FISHER, R., PUSZTAI, L. & SWANTON, C. (2013) Cancer heterogeneity: implications for targeted therapeutics. *Brit. J. Cancer*, **108**, 479–485.
- FRIEDL, P. & WOLF, K. (2003) Tumour-cell invasion and migration: diversity and escape mechanisms. *Nat. Rev. Cancer*, **3**, 362–374.

- GALLANT, N. D., MICHAEL, K. E. & GARCÍA, A. J. (2005) Cell adhesion strengthening: contributions of adhesive area, integrin binding, and focal adhesion assembly. *Mol. Biol. Cell*, **16**, 4329–4340.
- GEIGER, B. (1991) Long-range morphogenetic signals and cell adhesion. *BioEssays*, **13**, 665–666.
- GERISCH, A. & CHAPLAIN, M. A. J. (2008) Mathematical modelling of cancer cell invasion of tissue: local and non-local models and the effect of adhesion. *J. Theor. Biol.*, **250**, 684–704.
- GERISCH, A. & PAINTER, K. J. (2010) Mathematical modelling of cell adhesion and its applications to developmental biology and cancer invasion. *Cell Mechanics: From Single Scale-Based Models to Multiscale Modeling* (A. Chauviere, L. Preziosi & C. Verdier eds). Boca Raton, FL: Chapman & Hall/CRC, pp. 319–350.
- GOSWAMI, S., SAHAI, E., WYCKOFF, J. B., CAMMER, M., COX, D., PIXLEY, F. J., STANLEY, E. R., SEGALL, J. E. & CONDEELIS, J. S. (2005) Macrophages promote the invasion of breast carcinoma cells via a colony-stimulating factor-1/epidermal growth factor paracrine loop. *Cancer Res.*, **65**, 5278–5283.
- GREAVES, M. & MALEY, C. (2012) Clonal evolution in cancer. *Nature*, **481**, 306–313.
- GREEN, J. E. F., WATERS, S. L., WHITELEY, J. P., EDELSTEIN-KESHET, L., SHAKESHEFF, K. M. & BYRNE, H. M. (2010) Non-local models for the formation of hepatocyte-stellate cell aggregates. *J. Theor. Biol.*, **267**, 106–120.
- HAGEMANN, T., WILSON, J., KULBE, H., LI, N. F., LEINSTER, D. A., CHARLES, K., KLEMM, F., PUKROP, T., BINDER, C. & BALKWILL, F. R. (2005) Macrophages induce invasiveness of epithelial cancer cells via NF- κ B and JNK. *J. Immunol.*, **175**, 1197–1205.
- HANAHAN, D. & WEINBERG, R. A. (2000) The hallmarks of cancer. *Cell*, **100**, 57–70.
- HILL, R. P., CHAMBERS, A. F. & LING, V. (1984) Dynamic heterogeneity: rapid generation of metastatic variants in mouse B16 melanoma cells. *Science*, **224**, 998–1001.
- HÖFER, T., SHERRATT, J. A. & MAINI, P. K. (1995a) Cellular pattern formation during dictyostelium aggregation. *Phys. D: Nonlinear Phenomena*, **85**, 425–444.
- HÖFER, T., SHERRATT, J. A. & MAINI, P. K. (1995b) Dictyostelium discoideum: cellular self-organization in an excitable biological medium. *Proceedings of the Biological Sciences*, **259**, 249–257.
- HUNT, A. & SURULESCU, C. (2017) A multiscale modeling approach to glioma invasion with therapy. *Vietnam J. Math.*, **45**, 221–240.
- KEATS, J. J., CHESI, M., EGAN, J. B., GARBITT, V. M., PALMER, S. E., BRAGGIO, E., VAN WIER, S., BLACKBURN, P. R., BAKER, A. S., DISPENZIERI, A. *et al.* (2012) Clonal competition with alternating dominance in multiple myeloma. *Blood*, **120**, 1067–1076.
- KELKEL, J. & SURULESCU, C. (2012) A multiscale approach to cell migration in tissue networks. *Math. Models Methods Appl. Sci.*, **22**, 1150017.
- KHALIQUE, L., AYHAN, A., WEALE, M. E., JACOBS, I. J., RAMUS, S. J. & GAYTHER, S. A. (2007) Genetic intra-tumour heterogeneity in epithelial ovarian cancer and its implications for molecular diagnosis of tumours. *J. Pathol.*, **211**, 286–295.
- KIDERA, Y., TSUBAKI, M., YAMAZOE, Y., SHOJI, K., NAKAMURA, H., OGAKI, M., SATOU, T., ITOH, T., ISOZAKI, M., KANEKO, J. *et al.* (2010) Reduction of lung metastasis, cell invasion, and adhesion in mouse melanoma by statin-induced blockade of the Rho/Rho-associated coiled-coil-containing protein kinase pathway. *J. Exp. Clin. Cancer Res.*, **29**, 127.
- KNÚTSÐÓTTIR, H., PÁLSSON, E. & EDELSTEIN-KESHET, L. (2014) Mathematical model of macrophage-facilitated breast cancer cells invasion. *J. Theor. Biol.*, **357**, 184–199.
- LAIRD, A. K. (1964) Dynamics of tumor growth. *Brit. J. Cancer*, **18**, 490–502.
- LEITH, J. T., MICHELSON, S. & GLICKSMAN, A. S. (1989) Competitive exclusion of clonal subpopulations in heterogeneous tumours after stromal injury. *Brit. J. Cancer*, **59**, 22–27.
- LIN, E. Y., LI, J.-F., GNATOVSKIY, L., DENG, Y., ZHU, L., GRZESIK, D. A., QIAN, H., XUE, X.-N. & POLLARD, J. W. (2006) Macrophages regulate the angiogenic switch in a mouse model of breast cancer. *Cancer Res.*, **66**, 11238–11246.
- LING, S., HU, Z., YANG, Z., YANG, F., LI, Y., LIN, P., CHEN, K., DONG, L., CAO, L., TAO, Y. *et al.* (2015) Extremely high genetic diversity in a single tumor points to prevalence of non-Darwinian cell evolution. *Proceedings of the National Academy of Sciences*, **112**, E6496–E6505.

- LIU, J., HE, X., QI, Y., TIAN, X., MONKLEY, S. J., CRITCHLEY, D. R., CORBETT, S. A., LOWRY, S. F., GRAHAM, A. M. & LI, S. (2011) Talin1 regulates integrin turnover to promote embryonic epithelial morphogenesis. *Mol. Cell Biol.*, **31**, 3366–3377.
- LOBERT, V. H., BRECH, A., PEDERSEN, N. M., WESCHE, J., OPPELT, A., MALERØD, L. & STENMARK, H. (2010) Ubiquitination of $\alpha 5\beta 1$ integrin controls fibroblast migration through lysosomal degradation of fibronectin-integrin complexes. *Dev. Cell*, **19**, 148–159.
- LOEB, K. R. & LOEB, L. A. (2000) Significance of multiple mutations in cancer. *Carcinogenesis*, **21**, 379–385.
- LORENZ, T. & SURULESCU, C. (2014) On a class of multiscale cancer cell migration models: well-posedness in less regular function spaces. *Math. Models Methods Appl. Sci.*, **24**, 2383.
- MAHESHWARI, G., BROWN, G., LAUFFENBURGER, D. A., WELLS, A. & GRIFFITH, L. G. (2000) Cell adhesion and motility depend on nanoscale RGD clustering. *J. Cell Sci*, **113**, 1677–1686.
- MAREEL, M. M., DE BAETSELIER, P. & VAN ROY, F. M. (1991) *Mechanisms of Invasion and Metastasis*. Boca Raton, FL: CRC press.
- MARTELOTTO, L. G., NG, C. K., PISCUOGLIO, S., WEIGELT, B. & REIS-FILHO, J. S. (2014) Breast cancer intra-tumor heterogeneity. *Breast Cancer Res.*, **16**, 210.
- MARUSYK, A., ALMENDRO, V. & POLYAK, K. (2012) Intra-tumour heterogeneity: a looking glass for cancer? *Nat. Rev. Cancer*, **12**, 323–334.
- MARUSYK, A. & POLYAK, K. (2010) Tumor heterogeneity: causes and consequences. *Biochim. Biophys. Acta*, **1805**, 105.
- MEDLOCK, J. & KOT, M. (2003) Spreading disease: integro-differential equations old and new. *Math. Biosci.*, **184**, 201–222.
- MERAL, G., STINNER, C. & SURULESCU, C. (2015a) A multiscale model for acid-mediated tumour invasion: therapy approaches. *J. Coupled Systems Multiscale Dyn.*, **3**, 135–142.
- MERAL, G., STINNER, C. & SURULESCU, C. (2015b) On a multiscale model involving cell contractivity and its effects on tumour invasion. *J. Discrete Continuous Dyn. Systems - Series B.*, **20**, 189–213.
- MICHAEL, K. E., DUMBAULD, D. W., BURNS, K. L., HANKS, S. K. & GARCÍA, A. J. (2009) Focal adhesion kinase modulates cell adhesion strengthening via integrin activation. *Mol. Biol. Cell*, **20**, 2508–2519.
- MOGILNER, A., EDELSTEIN-KESHET, L. & ERMENTROUT, G. B. (1996) Selecting a common direction: II. Peak-like solutions representing total alignment of cell clusters. *J. Math. Biol.*, **34**, 811–842.
- MOGILNER, A. & EDELSTEIN-KESHET, L. (1995) Selecting a common direction: I. How orientational order can arise from simple contact responses between interacting cells. *J. Math. Biol.*, **33**, 619–660.
- MOGILNER, A. & EDELSTEIN-KESHET, L. (1999) A non-local model for a swarm. *J. Math. Biol.*, **38**, 534–570.
- MOLLISON, D. (1991) Dependence of epidemic and population velocities on basic parameters. *Math. Biosci.*, **107**, 255–287.
- MORANI, F., PHADNGAM, S., FOLLO, C., TITONE, R., THONGRAKARD, V., GALETTO, A., ALABISO, O. & ISIDORO, C. (2014) PTEN deficiency and mutant p53 confer glucose-addiction to thyroid cancer cells: impact of glucose depletion on cell proliferation, cell survival, autophagy and cell migration. *Genes Cancer*, **5**, 226–239.
- NESSYAHU, H. & TADMOR, E. (1990) Non-oscillatory central differencing for hyperbolic conservation laws. *J. Comput. Phys.*, **87**, 408–463.
- NICHOLSON, G. L. (1984) Cell surface molecules and tumor metastasis. Regulation of metastatic phenotypic diversity. *Exp. Cell Res.*, **150**, 3–22.
- NICHOLSON, G. L. (1987) Tumor cell instability, diversification and progression to the metastatic phenotype: from oncogene to oncofetal expression. *Cancer Res.*, **47**, 1473–1487.
- NOWELL, P. C. (1976) The clonal evolution of tumor cell populations. *Science*, **194**, 23–28.
- OTHMER, H., DUNBAR, S. & ALT, W. (1988) Models of dispersal in biological systems. *J. Math. Biol.*, **26**, 263–298.
- PAINTER, K., BLOOMFIELD, J., SHERRATT, J. & GERISCH, A. (2015) A nonlocal model for contact attraction and repulsion in heterogeneous cell populations. *Bull. Math. Biol.*, **77**, 1132–1165.
- PAINTER, K. J. (2009) Continuous models for cell migration in tissues and applications to cell sorting via differential chemotaxis. *Bull. Math. Biol.*, **71**, 1117–1147.

- PAINTER, K. J., ARMSTRONG, N. J. & SHERRATT, J. A. (2010) The impact of adhesion on cellular invasion processes in cancer and development. *J. Theor. Biol.*, **264**, 1057–1067.
- PERTHAME, B., TANG, M. & VAUCHELET, N. (2016) Derivation of the bacterial run-and-tumble kinetic equation from a model with biochemical pathway. *J. Math. Biol.*, **73**, 1161–1178.
- SCHUH, A., BECQ, J., HUMPHRAY, S., ALEXA, A., BURNS, A., CLIFFORD, R., FELLER, S. M., GROCOCK, R., HENDERSON, S., KHREBTUKOVA, I. *et al.* (2012) Monitoring chronic lymphocytic leukemia progression by whole genome sequencing reveals heterogeneous clonal evolution patterns. *Blood*, **120**, 4191–4196.
- SHAH, N. P., NICOLL, J. M., NAGAR, B., GORRE, M. E., PAQUETTE, R. L., KURIYAN, J. & SAWYERS, C. L. (2002) Multiple BCR-ABL kinase domain mutations confer polyclonal resistance to the tyrosine kinase inhibitor imatinib (STI571) in chronic phase and blast crisis chronic myeloid leukemia. *Cancer Cell*, **2**, 117–125.
- SHERRATT, J. A., GOURLEY, S. A., ARMSTRONG, N. J. & PAINTER, K. J. (2009) Boundedness of solutions of a non-local reaction-diffusion model for adhesion in cell aggregation and cancer invasion. *Eur. J. Appl. Math.*, **20**, 123–144.
- SHIAO, S.-Y. P. K. & OU, C.-N. (2007) Validation of oxygen saturation monitors in neonates. *Am. J. Crit. Care*, **16**, 168–178.
- STACKPOLE, C. W. (1983) Generation of phenotypic diversity in the B16 mouse melanoma relative to spontaneous metastasis. *Cancer Res.*, **43**, 3057–3065.
- STINNER, C., SURULESCU, C. & WINKLER, M. (2014) Global weak solutions in a PDE-ODE system modeling multiscale cancer cell invasion. *SIAM J. Math. Anal.*, **46**, 1969–2007.
- STINNER, C., SURULESCU, C. & MERAL, G. (2015) A multiscale model for pH-tactic invasion with time-varying carrying capacities. *IMA J. Appl. Math.*, **80**, 1300–1321.
- STINNER, C., SURULESCU, C. & UATAY, A. (2016) Global existence for a go-or-grow multiscale model for tumour invasion with therapy. *Math. Models Methods Appl. Sci.*, **26**, 2163.
- TOPAZ, C. M., BERTOZZI, A. L. & LEWIS, M. A. (2006) A nonlocal continuum model for biological aggregation. *Bull. Math. Biol.*, **68**, 1601–1623.
- WEITZMAN, J. B., CHEN, A. & HEMLER, M. E. (1995) Investigation of the role of $\beta 1$ integrins in cell-cell adhesion. *J. Cell Science*, **108**, 3635–3644.
- WOJCIECHOWSKA, S. & PATTON, E. E. (2015) Going forward together: cooperative invasion in melanoma. *Pigm. Cell Melanoma R.*, **28**, 6–7.
- XUE, C., HWANG, H., PAINTER, K. & ERBAN, R. (2011) Travelling waves in hyperbolic chemotaxis equations. *Bull. Math. Biol.*, **73**, 1695–1733.

Appendix A. Extension of the model to two dimensions

The derivation of the model in two dimensions is a straightforward extension of the methods used in Section 2.2. Let $\Omega \subset \mathbb{R}^2$ denote again the bounded spatial domain and $I_T = [0, +\infty)$ be the time interval. We only consider a rectangle with periodic boundary conditions. We denote again by $\underline{u}(\underline{x}, t) = (u_1(\underline{x}, t), u_2(\underline{x}, t))^T$ the vector-valued cancer cell density of the two populations, by $f(\underline{x}, t)$ the ECM density and by $c(\underline{x}, t)$ the integrin density. Our 2D system, obtained after non-dimensionalization, is given by

$$\frac{\partial u_1}{\partial t} = D\Delta u_1 - \nabla \cdot (u_1 \underline{F}_1[\underline{u}, f, c]) - Mu_1 + r_1 u_1 (1 - u_1 - u_2), \quad (\text{A.1a})$$

$$\frac{\partial u_2}{\partial t} = -\nabla \cdot (u_2 \underline{F}_2[\underline{u}, f, c]) + Mu_1 + r_2 u_2 (1 - u_1 - u_2), \quad (\text{A.1b})$$

$$\frac{\partial f}{\partial t} = -\alpha u_1 f - \beta u_2 f, \quad (\text{A.1c})$$

$$\frac{\partial c}{\partial t} = p_1 u_1 + p_2 u_2 - qc. \quad (\text{A.1d})$$

We now assume that cells interact with each other within a circle of sensing radius $R > 0$. Therefore, the nonlocal terms, $\underline{F}_i[\underline{u}, f, c]$, $i = 1, 2$, are given as in Gerisch & Chaplain (2008) by the following relations

$$\underline{F}_i[\underline{u}, f, c] := \frac{1}{R} \int_0^R \int_0^{2\pi} \underline{\eta}(\theta) K_i(r) g_i(\underline{u}(\underline{x} + r\underline{\eta}(\theta), t), f(\underline{x} + r\underline{\eta}(\theta), t), c(\underline{x}, t)) r \, d\theta \, dr, \quad (\text{A.2})$$

where $\underline{\eta}(\theta) := (\cos \theta, \sin \theta)^\top$ is the unit outer normal vector corresponding to angle θ . The functions g_i , $i = 1, 2$, are given by

$$g_i(\underline{u}(\underline{x}, t), f(\underline{x}, t), c(\underline{x}, t)) = S_i(c) u_i(\underline{x}, t) + S(c) u_j(\underline{x}, t) + C_i(c) f(\underline{x}, t), \quad i, j = 1, 2, \quad i \neq j. \quad (\text{A.3})$$

LINEAR STABILITY ANALYSIS FOR THE TWO DIMENSIONAL MODEL. Following the same approach as in the one-dimensional case (see Section 3), we analyse the stability of the steady states given by the relation (3.2). To this end, we let

$$\begin{aligned} u_1(\underline{x}, t) &= u_1^* + A_{u_1} e^{i\mathbf{k} \cdot \underline{x} + \lambda t}, \quad u_2(\underline{x}, t) = u_2^* + A_{u_2} e^{i\mathbf{k} \cdot \underline{x} + \lambda t}, \quad f(\underline{x}, t) = f^* + A_f e^{i\mathbf{k} \cdot \underline{x} + \lambda t}, \\ c(\underline{x}, t) &= c^* + A_c e^{i\mathbf{k} \cdot \underline{x} + \lambda t}, \quad \text{with } |A_{u_1}|, |A_{u_2}|, |A_f|, |A_c| \ll 1. \end{aligned}$$

Here, $\mathbf{k} = (k_1, k_2)$ is a perturbation wave vector and λ is the linear growth rate. Substituting these expressions into model (A1) we obtain the following linearized system:

$$\begin{aligned} \lambda A_{u_1} e^{i\mathbf{k} \cdot \underline{x} + \lambda t} &= -|\mathbf{k}|^2 D A_{u_1} e^{i\mathbf{k} \cdot \underline{x} + \lambda t} - \frac{u_1^*}{R} i\mathbf{k} e^{i\mathbf{k} \cdot \underline{x} + \lambda t} S_1(c^*) A_{u_1} \int_0^R \int_0^{2\pi} \underline{\eta}(\theta) K(r) e^{i\mathbf{k} \cdot r\underline{\eta}(\theta)} r \, d\theta \, dr \\ &\quad - \frac{u_1^*}{R} i\mathbf{k} e^{i\mathbf{k} \cdot \underline{x} + \lambda t} (S(c^*) A_{u_2} + C_1(c^*) A_f) \int_0^R \int_0^{2\pi} \underline{\eta}(\theta) K(r) e^{i\mathbf{k} \cdot r\underline{\eta}(\theta)} r \, d\theta \, dr \\ &\quad - M A_{u_1} e^{i\mathbf{k} \cdot \underline{x} + \lambda t} + r_1 A_{u_1} e^{i\mathbf{k} \cdot \underline{x} + \lambda t} (1 - 2u_1^* - u_2^*) - r_1 u_1^* A_{u_2} e^{i\mathbf{k} \cdot \underline{x} + \lambda t}, \\ \lambda A_{u_2} e^{i\mathbf{k} \cdot \underline{x} + \lambda t} &= -\frac{u_2^*}{R} i\mathbf{k} e^{i\mathbf{k} \cdot \underline{x} + \lambda t} (S_2(c^*) A_{u_2} + S(c^*) A_{u_1} + C_2(c^*) A_f) \int_0^R \int_0^{2\pi} \underline{\eta}(\theta) K(r) e^{i\mathbf{k} \cdot r\underline{\eta}(\theta)} r \, d\theta \, dr \\ &\quad + r_2 A_{u_2} e^{i\mathbf{k} \cdot \underline{x} + \lambda t} (1 - u_1^* - 2u_2^*) - r_2 u_2^* A_{u_1} e^{i\mathbf{k} \cdot \underline{x} + \lambda t}, \\ \lambda A_f e^{i\mathbf{k} \cdot \underline{x} + \lambda t} &= -\alpha (A_{u_1} e^{i\mathbf{k} \cdot \underline{x} + \lambda t} f^* + u_1^* A_f e^{i\mathbf{k} \cdot \underline{x} + \lambda t}) - \beta (A_{u_2} e^{i\mathbf{k} \cdot \underline{x} + \lambda t} f^* + u_2^* A_f e^{i\mathbf{k} \cdot \underline{x} + \lambda t}), \\ \lambda A_c e^{i\mathbf{k} \cdot \underline{x} + \lambda t} &= p_1 A_{u_1} e^{i\mathbf{k} \cdot \underline{x} + \lambda t} + p_2 A_{u_2} e^{i\mathbf{k} \cdot \underline{x} + \lambda t} - q A_c e^{i\mathbf{k} \cdot \underline{x} + \lambda t}. \end{aligned}$$

Therefore, we finally have

$$\begin{aligned} \lambda A_{u_1} &= -|\mathbf{k}|^2 D A_{u_1} - \frac{i\mathbf{k} u_1^*}{R} [S_1(c^*) A_{u_1} + S(c^*) A_{u_2} + C_1(c^*) A_f] \hat{\mathbf{K}}(\mathbf{k}) - M A_{u_1} + r_1 A_{u_1} (1 - 2u_1^* - u_2^*) \\ &\quad - r_1 u_1^* A_{u_2}, \\ \lambda A_{u_2} &= -\frac{i\mathbf{k} u_2^*}{R} [S_2(c^*) A_{u_2} + S(c^*) A_{u_1} + C_2(c^*) A_f] \hat{\mathbf{K}}(\mathbf{k}) + M A_{u_1} + r_2 A_{u_2} (1 - u_1^* - 2u_2^*) - r_2 u_2^* A_{u_1}, \\ \lambda A_f &= -\alpha (A_{u_1} f^* + u_1^* A_f) - \beta (A_{u_2} f^* + u_2^* A_f), \\ \lambda A_c &= p_1 A_{u_1} + p_2 A_{u_2} - q A_c, \end{aligned}$$

where $\hat{K}(\underline{k}) = \int_0^R \int_0^{2\pi} \underline{\eta}(\theta) K(r) e^{ikr\eta(\theta)} r \, d\theta \, dr$ is the Fourier transform of the kernel $K(\underline{x})$. Note that $\hat{K}(\underline{k})$ corresponds to the 1D Fourier sine transform (see Section 3), since $\hat{K}^s(k) = \int_0^R K(r) \sin(kr) \, dr = \frac{1}{2i} \int_0^R K(r) (e^{ikr} - e^{-ikr}) \, dr$.

As in 1D case, for the steady state $(0, 0, f^*, 0)$, $f^* \geq 0$, we obtain the eigenvalues

$$\lambda_1 = 0, \quad \lambda_2 = -|\underline{k}|^2 D - M + r_1, \quad \lambda_3 = r_2 > 0 \quad \text{and} \quad \lambda_4 = -q < 0. \quad (\text{A.4})$$

For the steady state $(0, 1, 0, p_2/q)$ we obtain the eigenvalues

$$\lambda_1 = -\beta < 0, \quad \lambda_2 = -|\underline{k}|^2 D - M < 0, \quad \lambda_3 = -S_2(c^*) Y(\underline{k}) - r_2 \quad \text{and} \quad \lambda_4 = -q < 0, \quad (\text{A.5})$$

where $Y(\underline{k}) = \frac{ik}{R} \hat{K}(\underline{k})$, with $K(\underline{x}) := q_a K_a(\underline{x}) - q_r K_r(\underline{x})$. Here K_a and K_r are the attraction and repulsion kernels, and q_a and q_r are the constants representing the magnitudes of the attraction and repulsion interactions, respectively. For simplicity we choose the following 2D interaction kernel

$$K(\underline{x}) = \frac{q_a |\underline{x}|}{2\pi m_a^2} \exp\left(-|\underline{x}|^2 / (2m_a^2)\right) - \frac{q_r |\underline{x}|}{2\pi m_r^2} \exp\left(-|\underline{x}|^2 / (2m_r^2)\right), \quad (\text{A.6})$$

which corresponds to the 1D kernel (3.15). The Fourier transform of the above kernel is given by the following relation

$$\hat{K}(\underline{k}) = \left(q_a i m_a^2 k_1 e^{-\frac{m_a^2 |k|^2}{2}} - q_r i m_r^2 k_1 e^{-\frac{m_r^2 |k|^2}{2}}, q_a i m_a^2 k_2 e^{-\frac{m_a^2 |k|^2}{2}} - q_r i m_r^2 k_2 e^{-\frac{m_r^2 |k|^2}{2}} \right). \quad (\text{A.7})$$

Therefore, the steady state $(0, 1, 0, p_2/q)$ is unstable provided that the real part of the eigenvalue λ_3 satisfies

$$\text{Re}(\lambda_3(\underline{k})) = -r_2 + \frac{|\underline{k}|^2 s_2^*}{R} \left(1 + \tanh\left(a_2 \frac{p_2}{q}\right) \right) \left(q_a m_a^2 e^{-\frac{m_a^2 |k|^2}{2}} - q_r m_r^2 e^{-\frac{m_r^2 |k|^2}{2}} \right) > 0. \quad (\text{A.8})$$

This expression is similar to the one obtained in the 1D case (see equation (3.17)). Therefore we deduce that there is a range of \underline{k} -values for which $\text{Re}(\lambda_3(\underline{k}))$ is positive, and thus spatial aggregations could develop also for the 2D model (A1) when applying small spatial perturbations of the steady state $(0, 1, 0, p_2/q)$.

Appendix B. A structured-population model for cancer–ECM interactions via integrins

As mentioned at the end of Section 2.1, we can modify model (2.13)–(2.16) to describe in a more natural way the connection between the macroscale movement of cells and the microscale dynamics of integrins bound to cell surfaces. To this end, we assume that the two cancer cell populations depend not only on time (t) and space (x), but also on an internal variable $c \geq 0$ that characterizes the level of bound integrins: $u_i(x, t, c)$. The new mesoscale model for the dynamics of cancer cell populations structured by cell-bound integrins is given by the following equations:

$$\frac{\partial u_1}{\partial t} = D \frac{\partial^2 u_1}{\partial x^2} - \frac{\partial}{\partial x} (u_1 F_1[\underline{u}, f, c]) - \frac{\partial}{\partial c} (u_1 (p_1 u_1 + p_2 u_2 - qc)) - M u_1 + r_1 u_1 (1 - u_1 - u_2), \quad (\text{B.1a})$$

$$\frac{\partial u_2}{\partial t} = -\frac{\partial}{\partial x} (u_2 F_2[\underline{u}, f, c]) - \frac{\partial}{\partial c} (u_2 (p_1 u_1 + p_2 u_2 - qc)) + M u_1 + r_2 u_2 (1 - u_1 - u_2), \quad (\text{B.1b})$$

$$\frac{\partial f}{\partial t} = -\alpha u_1 f - \beta u_2 f. \quad (\text{B.1c})$$

The nonlocal terms $F_1[\underline{u}, f, c]$ and $F_2[\underline{u}, f, c]$ are described by equations (2.10) and (2.11), respectively. The microscale evolution of the internal state variable c is described by differential equation (2.16):

$$\frac{\partial c}{\partial t} = p_1 u_1 + p_2 u_2 - qc. \quad (\text{B.2})$$

The incorporation of this internal cell structure c into the mesoscopic model (B1) follows the same approach as in Erban & Othmer (2004, 2005); Xue *et al.* (2011); Lorenz & Surulescu (2014); Engwer *et al.* (2015); Perthame *et al.* (2016); Engwer *et al.* (2017); Hunt & Surulescu (2017).

One can eliminate the derivative $\partial/\partial c$ from equations (B1a)–(B1b) by integrating these equations over c , and obtaining new macroscopic equations defined in terms of the averaged tumour cell variables $U_{1,2}(x, t) = \int u_{1,2}(x, t, c) dc$ (Erban & Othmer, 2005; Engwer *et al.*, 2015; Domschke *et al.*, 2107). Other studies obtained different macroscopic limits of the mesoscopic structured-population models by considering the assumption that the internal (structure) variable evolves on a much faster time scale that is described by a small parameter ε (Perthame *et al.*, 2016). If we would take the same approach and assume that the integrin dynamics is much faster compared to the dynamics of cancer cells and ECM (note that in Table 2 the production rates of integrins by u_1 and u_2 cells are estimated, due to a lack of available data), then the time-evolution of integrins would be given by

$$\varepsilon \frac{\partial c}{\partial t} = p_1 u_1 + p_2 u_2 - qc, \quad (\text{B.3})$$

which, to leading order, gives rise to the following steady-state equation: $c = (1/q)(p_1 u_1(x) + p_2 u_2(x))$. If we substitute this state into (B1) we recover model (2.22), with the exception of equation (2.22d) which is now a steady-state equation.

We note here that while different ‘microscale–macroscale’ models (Stinner *et al.*, 2014, 2015, 2016; Meral *et al.*, 2015a,b) and ‘mesoscale’ models (Lorenz & Surulescu, 2014; Engwer *et al.*, 2015; Perthame *et al.*, 2016; Engwer *et al.*, 2017; Hunt & Surulescu, 2017) for tumour-ECM interactions via integrins have been developed over the last two decades, to our knowledge there are not many studies that compare and contrast the outcomes of different ways the integrins are incorporated into these different models.

A comparison between the effects of integrins on the dynamics of the structured-population model (B1) and the original model (2.22) (both assuming heterogeneous cell populations), including an investigation into the possibility of having travelling wave solutions for the structured model (B1), will be the subject of a future study. (Such an investigation is beyond the scope of this study due to its complexity, which would increase considerably the length of this paper.)